

# Comparative evaluation of earthquake forecasting models: An application to Italy

**Jonas R. Brehmer**

Heidelberg Institute for Theoretical Studies

**Kristof Kraus** and **Tilmann Gneiting**

Heidelberg Institute for Theoretical Studies

Karlsruhe Institute of Technology (KIT)

**Marcus Herrmann** and **Warner Marzocchi**

University of Naples, Federico II

May 20, 2024

## Abstract

Testing earthquake forecasts is essential to obtain scientific information on forecasting models and sufficient credibility for societal usage. We aim at enhancing the testing phase proposed by the Collaboratory for the Study of Earthquake Predictability (CSEP, [Schorlemmer et al., 2018](#)) with new statistical methods supported by mathematical theory. To demonstrate their applicability, we evaluate three short-term forecasting models that were submitted to the CSEP Italy experiment, and two ensemble models thereof. The models produce weekly overlapping forecasts for the expected number of M4+ earthquakes in a collection of grid cells. We compare the models' forecasts using consistent scoring functions for means or expectations, which are widely used and theoretically principled tools for forecast evaluation. We further discuss and demonstrate their connection to CSEP-style earthquake likelihood model testing. Then, using tools from isotonic regression, we investigate forecast reliability and apply score decompositions in terms of calibration and discrimination. Our results show where and how models outperform their competitors and reveal a substantial lack of calibration for various models. The proposed methods also apply to full-distribution (e. g., catalog-based) forecasts, without requiring Poisson distributions or making any other type of parametric assumption.

*Keywords.* Calibration; earthquake count; forecast evaluation; reliability diagram; scoring function.

## 1 Introduction

Earthquake forecasting has broad, manifold impact: It demarcates the interface between seismology and society, being the basic scientific component of any sound seismic risk reduction strategy; simultaneously, it is the ultimate scientific challenge for seismologists, because it allows testing different hypotheses about earthquake occurrence processes.

Owing to the physical complexity of earthquake occurrence and our lack of knowledge, earthquake forecasts are unavoidably probabilistic, meaning they provide the full or parts of the predictive distribution of future seismicity. To be of scientific and practical use, the earthquake forecasting enterprise must be intimately linked to a solid testing

phase, which allows seismologists to evaluate the reliability and predictive performance of the forecasts and give them the necessary credibility they need for societal purposes. Enhancing the testing phase of earthquake forecasts is the main motivation of this paper.

Presently, several flavors of physics-based (e.g., [Cattania et al., 2018](#); [Mancini et al., 2019](#); [Sharma et al., 2020](#); [Dahm and Hainzl, 2022](#)) or statistical (e.g., [Gerstenberger et al., 2005](#); [Falcone et al., 2010](#); [Lombardi and Marzocchi, 2010](#); [Woessner et al., 2010](#); [Bayliss et al., 2020](#)) models exist that issue such forecasts. To date, the most common methods to evaluate the resulting model output are set by the *Collaboratory for the Study of Earthquake Predictability* (CSEP) and rely on standardized prospective tests. Prospective tests only use data gathered after the model was submitted to an experiment. CSEP is a continuously evolving enterprise, both in the format of the forecasts and in the set of tests. To preserve transparency and replicability, CSEP maintains the original models' forecasts and related data to allow any scientist to re-run the experiment with, for example, an updated set of tests. A key part of the CSEP testing strategy is an approach that can be broadly termed *earthquake likelihood model testing* ([Kagan and Jackson, 1995](#); [Schorlemmer et al., 2007](#)). In its original format, it partitions the testing region into grid cells and assigns a *log likelihood* to each forecast, which comprises Poisson log likelihoods for observed counts of earthquakes. Although similar in form, the approach differs in crucial aspects from widely used statistical out-of-sample forecast evaluation methods developed for count data in other scientific fields ([Czado et al., 2009](#); [Kolassa, 2016](#)). More importantly, the log likelihood-based tests lack a formal mathematical theory.

In this paper we aim at filling this gap, providing additional statistical procedures that are deeply rooted in probability theory to evaluate and compare earthquake forecasts. Specifically, we build on recent advances in [Brehmer et al. \(2024\)](#) and illustrate how CSEP's log likelihood-based testing method is related to consistent scoring (or loss) functions, which are well-established tools from decision theory to compare forecast performance ([Gneiting and Raftery, 2007](#); [Gneiting, 2011](#)). Furthermore, we introduce methods proposed by [Gneiting and Resin \(2023\)](#) to investigate a model's reliability, and we apply score decompositions in terms of calibration and discrimination capabilities. We use the newly proposed tools to compare and analyze five forecasting models regarding the operational earthquake forecasting (OEF) system in Italy ([Marzocchi et al., 2014](#)). The final goal is to propose additional mathematical resources that may make the CSEP testing phase stronger.

Technical settings and terminology matter, and to create an effective bridge between different fields, here seismology and mathematics, we need to pay attention to fundamental concepts and terminology of the mathematical theory used, starting with the details of the forecast format. Specifically, we consider forecasts of the number of earthquakes in a given space–time–magnitude bin. As argued by [Nandan et al. \(2019\)](#), forecasting models ought to embrace the full distribution of the number of earthquakes. However, a full-distribution forecast can always be reduced to its mean or expected value, and it is this simplified format on which we focus here. Thus, the forecast is a nonnegative real number, which represents a mean or expected count, and the respective outcome is

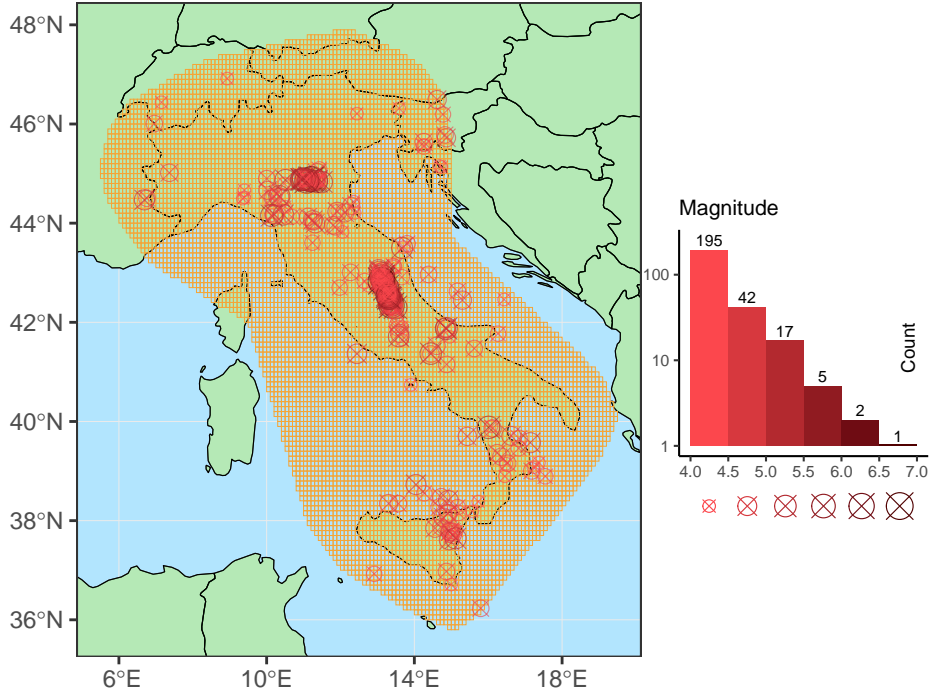


Figure 1: Left: Forecast region of OEF-Italy (orange grid, 8993 grid cells, which corresponds to the testing region of the Italian CSEP experiment) and locations of observed M4+ target earthquakes (crossed circles) between 2005 April 16 and 2020 May 20; Right: Logarithmic bar plot of earthquake magnitudes. For similar displays, see Figure 1 of [Herrmann and Marzocchi \(2023\)](#), Figure 1 of [Spassiani et al. \(2023\)](#), and Figure 2 of [Brehmer et al. \(2024\)](#).

the observed count, which is a nonnegative integer. Evidently, short-term earthquake forecasts operate within a *low probability* ([Jordan et al., 2011](#)) or *low count* environment, where an overwhelming majority of the observed counts is zero. [Serafini et al. \(2022\)](#) and [Spassiani et al. \(2023\)](#) consider an even simpler format, namely that of probability forecasts for the binary event of at least one target earthquake occurring in any given space–time–magnitude bin, to which we also relate. The setting of single-valued forecasts in the form of an expected count or number, on which we focus in this paper, fits current practice at CSEP and allows for comprehensive comparisons.

Figure 1 depicts the Italian CSEP testing region in which the five models produce forecasts in the form of the expected number of earthquakes in space–time–magnitude bins. We term the first two models as LM ([Lombardi and Marzocchi, 2010](#)) and FCM ([Falcone et al., 2010](#)). Both are ETAS models, but with customized structure and calibration choices. The third model, termed LG ([Lolli and Gasperini, 2003](#); [Woessner et al., 2010](#)), is based on the short-term earthquake probability (STEP) model ([Gerstenberger](#)

et al., 2005). These three models were evaluated in the Italian CSEP experiment (Taroni et al., 2018, providing one-day ahead forecasts). The fourth model, SMA, is a weighted-average ensemble of the previous three models and used in OEF-Italy (Marzocchi et al., 2014); its weights are proportional to the inverse of the log likelihood of the observed data following the score model averaging (SMA) rule and are continuously updated with new observations. We additionally include a further weighted-average ensemble of the three candidates, termed LRWA (Herrmann and Marzocchi, 2023), where the weighting is based on logistic regression (specifically, the variant fit to M3+ earthquakes with fitting scheme #2, see their Appendix C).

The models issue forecasts in the form of the expected number of earthquakes with magnitudes equal to or larger than four (M4+, the target threshold) in the next seven days for each of the 8993 spatial grid cells of the testing region. On any given day, the forecast is a collection of 8993 positive values which we denote via  $x_{c,t}^{(j)}$ , where  $j$  represents the model,  $c$  the grid cell, and  $t$  the day. To evaluate these forecasts, we consider M4+ target earthquakes that occurred between 2005 April 16 and 2020 May 26 in the testing region. This yields 5520 days in total and results in 5514 forecast–observation pairs. The observations  $y_{c,t}$  represent the number of M4+ target earthquakes in grid cell  $c$  during the seven-day period starting at  $t$ , and become available after day  $t + 6$ .

The models issue forecasts at 00:00 on each day and immediately after M3.5+ earthquakes. We do not consider the latter (intra-day) runs and thus obtain an equally spaced sequence of forecasts in time. A crucial benefit of the expected counts format is that forecasts can be aggregated spatially,<sup>1</sup> as visualized in Figure 2, where at top we plot spatially aggregated forecasts. We see that the models vary in several dimensions. The respective forecasts have different background levels (top, bottom) and feature distinct spatial smoothness (bottom), though they are strongly correlated with each other. In the next two sections we focus on terminology and theoretical concepts, but also provide extensive analyses and demonstrations based on these forecasts.

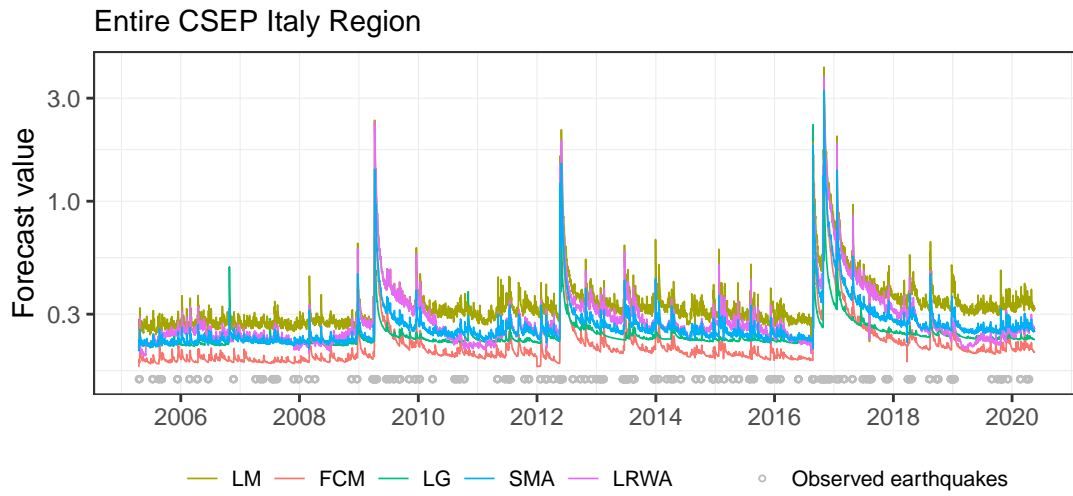
## 2 Comparative evaluation via consistent scoring functions

Consistent scoring functions are mathematically principled tools for the overall evaluation, comparison, and ranking of competing forecast models. We take scoring functions to be negatively oriented penalties that a forecaster wishes to minimize. In a nutshell, if the forecast posits an expected count  $x$  and the count  $y$  realizes, the penalty is  $S(x, y)$ . In practice, scores are suitably averaged.

For instance, in the setting of OEF-Italy, which spatially coincides with the testing region of the Italian CSEP experiment, there are  $C = 8993$  grid cells and  $T = 5514$  test days. The *total score* of model  $j$  over the testing region and testing period from Figure

---

<sup>1</sup>The aggregation is simply by summation. For example, the expected count for the entire CSEP testing region equals the sum of the expected counts for the 8993 grid cells. In contrast, full-distribution forecasts do not allow for linear nor other straightforward types of aggregation from bins.



### Seven-Day Period Starting 2005 April 16

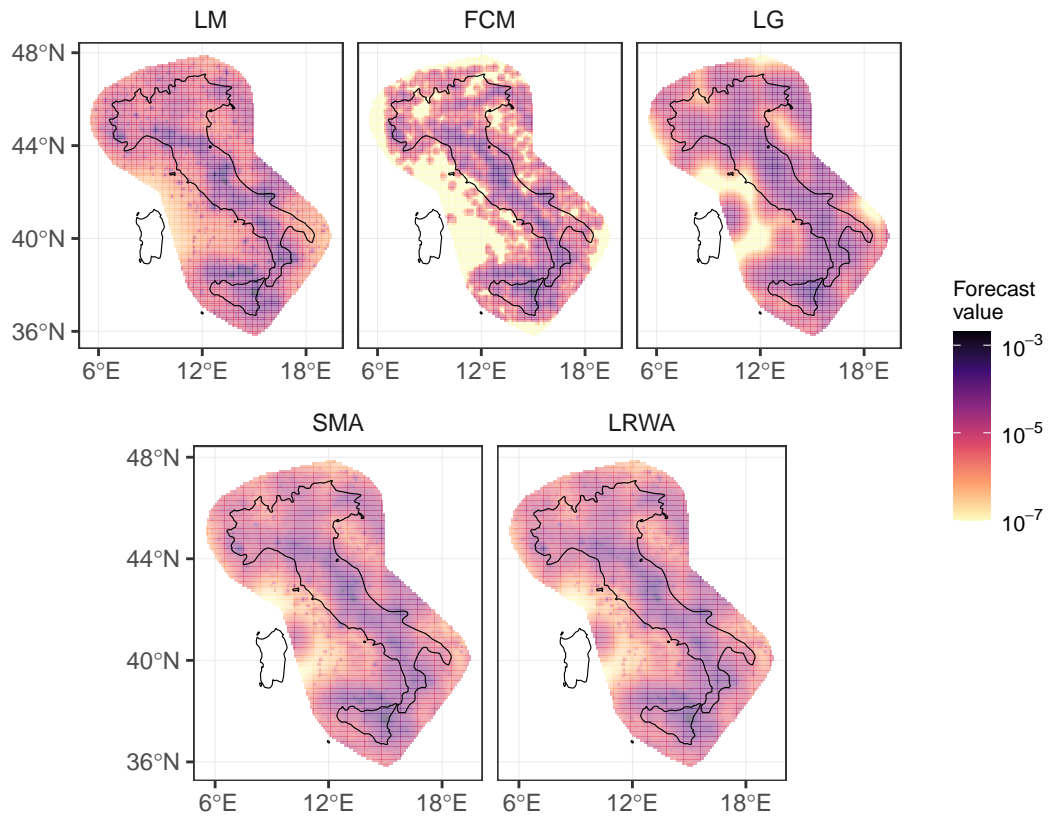


Figure 2: Top: Expected number forecasts aggregated over the testing region for each day; Bottom: Expected number forecasts of  $10^{-7}$  and higher for the initial seven-day period in OEF-Italy.

1 is

$$\bar{S}^{(j)} = \frac{1}{T} \sum_{t=1}^T \bar{S}_t^{(j)}, \quad (1)$$

where

$$\bar{S}_t^{(j)} = \sum_{c=1}^C \mathfrak{S}\left(x_{c,t}^{(j)}, y_{c,t}\right) \quad (2)$$

is the spatially aggregated score for model  $j$  on day  $t$ . Considering all  $C$  grid cells and  $T$  days, the total score considers  $n = C \times T = 8993 \times 5514$  individual forecast cases in OEF-Italy. Note that we use summation rather than averaging to define the spatially aggregated score at (2), as the summation yields numerical values that are convenient to report, compare, and interpret.

A key question then is which scoring function ought to be used, and we emphasize that the choice needs to be mathematically consistent with the scope and format of the forecast, which represents the *a priori* mean or expected number of earthquakes. Despite our focus on forecasts in the form of expected counts, it is instructive to begin the discussion in the setting of full-distribution forecasts.

## 2.1 Proper scoring rules for full-distribution forecasts

To fix the idea, let  $P$  be a full-distribution forecast for count data, such as the number of earthquakes in a space–time–magnitude bin. Evidently,  $P$  is a probability distribution on the set of the nonnegative integers. We adopt notation from [Czado et al. \(2009\)](#) and denote its probability mass function by  $(p_k)_{k=0}^{\infty}$  and the respective cumulative distribution function (CDF) by  $(P_k)_{k=0}^{\infty}$ , where  $P_k = \sum_{j=0}^k p_j$  for any integer  $k \geq 0$ .

In this setting, a scoring rule  $R(P, y)$  assigns a penalty based on the full-distribution forecast  $P$  and the corresponding observed count  $y$ . The scoring rule  $R$  ought to be such that

$$\mathbb{E}_{Y \sim Q} R(Q, Y) \leq \mathbb{E}_{Y \sim Q} R(P, Y), \quad (3)$$

where  $\mathbb{E}$  denotes the expectation operator,  $P$  and  $Q$  are full-distribution forecasts, and  $Y$  is a random variable with distribution  $Q$ . Indeed, if  $Q$  is the true (though typically unknown) distribution of the count, then the full-distribution forecast  $Q$  ought to outperform any other forecast  $P$  in expectation. A scoring rule for which the expectation inequality in (3) is true for all  $P, Q$  in a class  $\mathcal{P}$  of probability distributions is said to be *proper* relative to  $\mathcal{P}$ . If equality in (3) occurs only when  $P = Q$ , the scoring rule is *strictly proper*. Propriety is an essential characteristic of a scoring rule which encourages honest and coherent forecasts ([Gneiting and Raftery, 2007](#)) and ensures that appropriate and complete usage of information is rewarded ([Holzmann and Eulert, 2014](#)).

Key examples of proper scoring rules for count data include the *logarithmic* score, which is defined as

$$R(P, y) = -\log p_y \quad (4)$$

and depends on the forecast  $P$  only through the probability mass  $p_y$  at the observed count, and the *ranked probability score*,

$$R(P, y) = \sum_{k=0}^y P_k^2 + \sum_{k=y+1}^{\infty} (1 - P_k)^2 = \mathbb{E}_{Y \sim P} |Y - y| - \frac{1}{2} \mathbb{E}_{Y \sim P} |Y - Y'|, \quad (5)$$

where  $Y$  and  $Y'$  are independent copies of a random variable with distribution  $P$ . The representation at right holds whenever the distribution  $P$  has a finite (as opposed to infinite) expected value, and it demonstrates that the ranked probability score can be interpreted in terms of (fractional) counts. [Czado et al. \(2009\)](#) and [Kolassa \(2016\)](#) provide detailed discussions of these and other proper scoring rules.

## 2.2 Consistent scoring functions for expected counts

In the context of forecasts of a mean or expected count, consistency is the equivalent of propriety ([Savage, 1971](#); [Gneiting, 2011](#)). Specifically, let  $\mathcal{P}$  be the class of probability distributions on the nonnegative integers with finite mean or expectation, and let  $P \in \mathcal{P}$  have expectation  $\mu_P$ . The scoring function  $S$  is *consistent* for forecasts of an expected count if

$$\mathbb{E}_{Y \sim P} S(\mu_P, Y) \leq \mathbb{E}_{Y \sim P} S(x, Y) \quad (6)$$

for all distributions  $P \in \mathcal{P}$  and nonnegative numbers  $x$ . The scoring function is *strictly consistent* if equality in (6) implies  $x = \mu_P$ . Consistency ensures that reporting the truth is an optimal strategy when forecasters are rewarded according to their realized scores, and strict consistency guarantees that the true expectation  $\mu_P$  is the only minimizer of the expected score  $\mathbb{E}_{Y \sim P} S(x, Y)$ . Hence, a forecast is preferred over its competitors if it achieves lower average scores. To see the connection to strictly proper scoring rules, we note that if  $S(x, y)$  is a consistent scoring function in the sense of Eq. (6) then  $R(P, y) = S(\mu_P, y)$  is a proper scoring rule for full-distribution forecasts in the sense of Eq. (3).<sup>2</sup>

Due to the condition (6) prescribed by consistency, it is an intricate question what consistent scoring functions are available for expected counts. Summarizing results originally due to [Savage \(1971\)](#) and reviewed by [Gneiting \(2011\)](#) and [Brehmer et al. \(2024\)](#), among others, the (strictly) consistent scoring functions for an expected count are of the form

$$S(x, y) = \phi(y) - \phi(x) - \phi'(x)(y - x) + h(y), \quad (7)$$

where  $x \geq 0$ ,  $y \in \{0, 1, \dots\}$ ,  $\phi$  is a (strictly) convex function,  $\phi'$  is a subgradient of  $\phi$ , and  $h$  is an essentially arbitrary function.<sup>3</sup>

<sup>2</sup>Indeed, if  $P, Q \in \mathcal{P}$  then  $\mathbb{E}_{Y \sim Q} R(Q, Y) = \mathbb{E}_{Y \sim Q} S(\mu_Q, Y) \leq \mathbb{E}_{Y \sim Q} S(\mu_P, Y) = \mathbb{E}_{Y \sim Q} R(P, Y)$ , which demonstrates the claim.

<sup>3</sup>A subgradient is a generalization of a derivative; whenever a derivative exists, the subgradient is unique and coincides with the derivative. For further technical discussion we refer to Section 3.1 of [Gneiting \(2011\)](#), Section 2 of [Brehmer et al. \(2024\)](#), and Appendix A.1 in this current paper.

Table 1: Predictive performance of forecast models for OEF-Italy in terms of the average score  $\bar{S}$  from (1) under the Poisson scoring function at (9) and the quadratic scoring function at (8). The best (lowest) score in each column is highlighted in green.

Score	Poisson	Quadratic
LM	2.71	0.8407
FCM	2.80	0.8459
LG	3.02	0.8465
SMA	2.73	0.8437
LRWA	2.69	0.8421

The most prominent example of a strictly consistent scoring function for an expected value in the scientific literature is the *quadratic* scoring function

$$S_{\text{quad}}(x, y) = (x - y)^2, \quad (8)$$

which arises from  $\phi(x) = x^2$  and  $h(y) = 0$  in (7). This function is symmetric in the sense that  $S_{\text{quad}}(x, y) = S_{\text{quad}}(y, x)$ . Another valid choice of a convex function in (7) is  $\phi(x) = x(\log x - 1)$ . Taking  $h(y) = -\phi(y)$ , this yields the *Poisson* scoring function  $S_{\text{pois}}$  defined by

$$S_{\text{pois}}(x, y) = x - y \log x \quad (9)$$

for expected counts  $x > 0$  and observed numbers  $y \in \{0, 1, \dots\}$  of earthquakes, which also is strictly consistent. The case  $x = 0$  does not occur in typical practice, but can be handled by assigning  $S_{\text{pois}}(0, 0) = 0$  and  $S_{\text{pois}}(0, y) = +\infty$  for  $y \in \{1, 2, \dots\}$ .

For a connection to proper scoring rules, note that the logarithmic score at (4) recovers the Poisson score at (9) when  $p_y$  is the probability mass of a Poisson distribution with rate  $x > 0$ , save for terms that depend on the outcome  $y$  only. In other words,  $S_{\text{pois}}(x, y)$  corresponds to the log likelihood of a Poisson distributed random variable and therefore is equivalent to the main evaluation function used in the earthquake likelihood model testing approach (Schorlemmer et al., 2007). However, the connection is purely formal, and the use of the Poisson scoring function neither explicitly nor implicitly requires Poisson distributions or any other type of parametric assumptions, as pointed out by Brehmer et al. (2024). Both the quadratic and the Poisson scoring function are members of the *extended Patton family*, which is an extension to count data of the scoring functions proposed by Patton (2011). For details see Appendix A.2.

As Table 1 shows, the quadratic score and the Poisson score yield distinct rankings of the five models. Under the quadratic scoring function, the LM model has the best (lowest) score; under the Poisson scoring function the LRWA model shows the lowest score.<sup>4</sup> As there are many strictly consistent scoring functions, it is unclear whether conclusions are reasonably stable with respect to the choice of scoring function. In

<sup>4</sup>Differences between Tables 1–3 in this current paper and Table 1 in Brehmer et al. (2024), as well as between Table 3 and Table 1 in Herrmann and Marzocchi (2023), stem from a corrected spatial



investigating this stability, we rely on an alternative characterization of scoring functions from [Ehm et al. \(2016\)](#). To this end, we define the *elementary* scoring function  $S_\theta$  with threshold parameter  $\theta > 0$ , namely,

$$S_\theta(x, y) = \begin{cases} 0, & x, y \leq \theta \text{ or } x, y \geq \theta, \\ |y - \theta|, & \text{otherwise,} \end{cases} \quad (10)$$

which arises from the classical representation (7) by choosing the convex function  $\phi(x) = \max(x - \theta, 0)$  and  $h(y) = 0$ . Thus,  $S_\theta$  assigns a score of zero if the expected number  $x$  and the observed count  $y$  lie on the same side of  $\theta$ , and a score that equals the distance between  $y$  and  $\theta$  otherwise. We note that  $S_\theta$  is a consistent, but not a strictly consistent scoring function since  $x = y$  is not the only minimizer of the score.

Remarkably,  $S_\theta$  represents a cost–benefit scenario in a stylized decision problem with a decision threshold at  $\theta$ , where  $\theta$  can be interpreted as the ratio of the socio-economic cost of a preventive measure under consideration, such as an evacuation, over the (monetized) benefit (per earthquake) of the measure, e.g., the number of saved human lives (per earthquake). If the expected number of earthquakes  $x$  lies below the threshold  $\theta$ , the induced optimal decision is to take no action; if  $x$  is above  $\theta$ , the induced optimal decision is to apply the preventive measure.<sup>5</sup> In this scenario  $S_\theta(x, y)$  at (10) is proportional to the difference of the cost or loss under the optimal decision induced by the forecast  $x$  and the (hypothetical) cost under the optimal decision in hindsight ([Ehm et al., 2016](#), Section 3.1). Notwithstanding the crude simplifications in the stylized decision problem, decision thresholds (only) take (very) small positive values in practical problems of short-term forecasts of damaging earthquakes.

The results of [Ehm et al. \(2016\)](#) imply that subject to modest regularity conditions, a consistent scoring function  $S$  for an expected count admits a representation of the form

$$S(x, y) = \int_0^\infty S_\theta(x, y) w(\theta) d\theta, \quad (11)$$

where  $w(\theta)$  is a non-negative weight function that assigns relevance to the threshold parameter  $\theta > 0$  for the elementary scoring function  $S_\theta$  from (10). As noted by [Taggart \(2022, p. 306\)](#), the score is “the weighted average of economic regret over user decision thresholds, where the weight emphasises those decision thresholds in the corresponding region of interest.” The scoring function  $S$  in (11) is strictly consistent if the weight function  $w(\theta)$  is strictly positive. If we put  $h(x) = 0$ , then the convex function  $\phi$  in the classical representation (7) and the weight function  $w$  in the nearly equivalent, but more interpretable, representation (11) relate to each other in simple ways. Specifically, if  $\phi$  admits a second derivative  $\phi''$ , then  $w(\theta) = \phi''(\theta)$  for  $\theta > 0$ . For example, the quadratic scoring function at (8) arises from the choice  $\phi(x) = x^2$ , which yields the uniform weight function  $w(\theta) = \phi''(\theta) = 2$  for  $\theta > 0$ , so all values of the decision threshold  $\theta$  are

---

binning of earthquakes that occurred exactly on grid cell boundaries. Details are available at [https://github.com/jbrehmer42/Earthquakes\\_Italy](https://github.com/jbrehmer42/Earthquakes_Italy).

<sup>5</sup>Let  $c$  be the socio-economic cost of the preventive measure, and let  $b$  denote its monetized benefit per earthquake. Then the measure ought to be undertaken if  $bx > c$  or  $x > c/b = \theta$ .

weighted equally. The Poisson scoring function at (9) arises from the convex function  $\phi(x) = x(\log x - 1)$ , which yields the corresponding weight function  $w(\theta) = \phi''(\theta) = \theta^{-1}$  for  $\theta > 0$ , so small positive values of the decision threshold  $\theta$  receive dominant weights. Importantly, this analysis demonstrates that in the setting of earthquake forecasting, the Poisson scoring function with its emphasis on small positive decision thresholds is more relevant than the quadratic scoring function.

To investigate how forecast performance depends on the choice of the consistent scoring function, we can plot a Murphy diagram. In the original form proposed by Ehm et al. (2016), the Murphy diagram plots the average score (1) under the elementary scoring function  $S_\theta$  from (10) for the model(s) at hand as a function of the threshold parameter  $\theta$ . Here we adapt the Murphy diagram to the low probability and low count setting of earthquake forecasts and introduce the *logarithmic Murphy diagram*, where we plot against  $\log \theta$ . Conveniently, the integral under a model’s logarithmic Murphy curve equals its average Poisson score.<sup>6</sup> If a model has lower average elementary scores than its competitors for all choices of the threshold parameter  $\theta$ , then it has superior forecast performance with respect to all strictly consistent scoring functions for the mean.

Figure 3 shows a logarithmic Murphy diagram for the five OEF-Italy forecast models. It is interesting to observe that each of the five models has certain ranges of  $\theta$  under which it performs best in terms of the average score under  $S_\theta$ . The LM model shows outstanding performance at larger values of  $\theta$  and thus has the smallest average score under the quadratic scoring function, which gives equal weight to all values of  $\theta$ . The LRWA ensemble model shows excellent performance across all values of  $\log \theta$  and has the smallest average score under the Poisson scoring function. As we have argued, the Poisson scoring function emphasizes performance at small values of  $\theta$  that societally are the most relevant, and a model’s average Poisson score equals the area under the logarithmic Murphy curve.

### 2.3 The Diebold–Mariano test of equal predictive ability

Worthy of note, scoring functions rank the forecast models’ performance, but to make formal statistical inference, additional procedures and assumptions are required. To check for statistically significant differences in forecast performance, we consider tests of the (null) hypothesis of equal predictive performance for two models in terms of a given scoring function  $S$ . For this purpose, we make use of the Diebold–Mariano test, which is a carefully adapted Student- $t$  two-sample test (Diebold and Mariano, 1995; Gneiting and Katzfuss, 2014, Section 3.1).

Specifically, we consider the daily scores  $\bar{S}_t^{(j)}$  and  $\bar{S}_t^{(k)}$  of models  $j$  and  $k$  on day  $t$  from (2), which are obtained after spatial aggregation, with the individual scores for the grid cells summed up, and summarize forecast performance over the whole testing region for one seven-day forecast period. The top panel in Figure 4 shows these daily scores based

---

<sup>6</sup>The claim follows immediately from our discussion of the representation (11) for the Poisson scoring function and the fact that  $\int \bar{S}_\theta d(\log \theta) = \int \bar{S}_\theta \theta^{-1} d\theta$ . The average score (1) under the elementary scoring function  $S_\theta$  at (10) is identically zero for sufficiently small and sufficiently large values of  $\theta$ , so the integral is guaranteed to be finite.

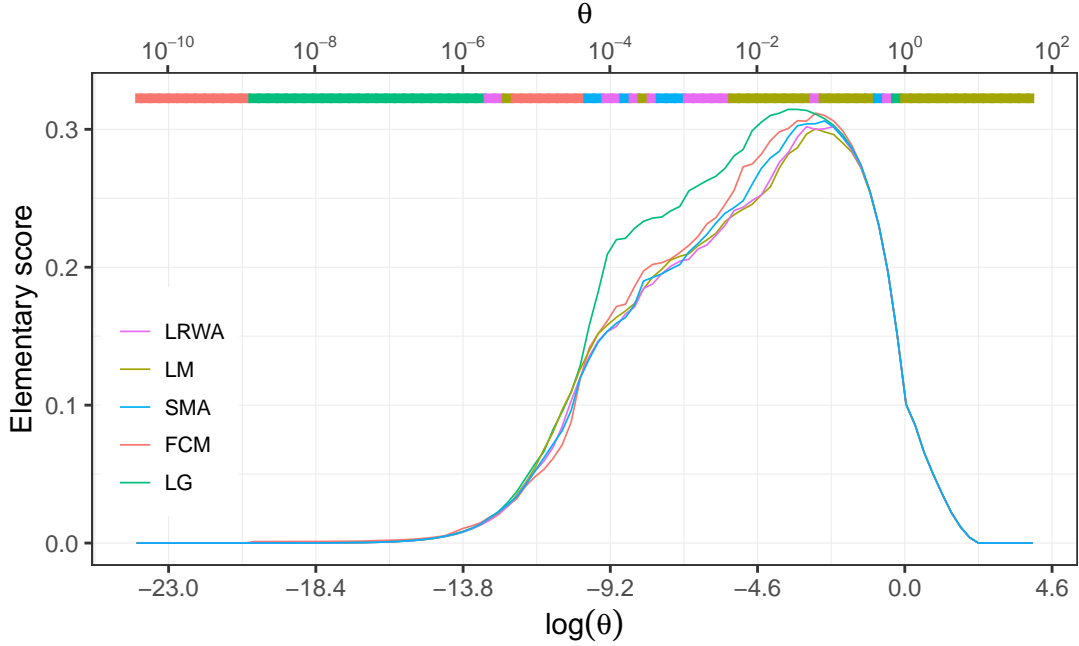


Figure 3: Logarithmic Murphy diagram for the five forecast models. Each curve plots a model’s total elementary score  $\bar{S}_\theta$  from (1) versus  $\log \theta$ . Tickmarks at bottom indicate  $\log \theta$ ; tickmarks at top show  $\theta$ . The colored bar at top indicates the model with the lowest value of  $\bar{S}_\theta$ . The integral under a model’s curve equals the average Poisson score from Table 1.

on the Poisson scoring function  $S_{\text{pois}}$  for the five forecast models. It uses a logarithmic scale, because the daily scores are much larger for forecast periods  $t$  that contain M4+ target earthquakes, corresponding to counts  $y_{c,t} \geq 1$  for at least one grid cell  $c$ . The LM model generally performs worst on forecast periods without M4+ earthquakes, as it possesses the highest daily scores for such  $t$ , and frequently performs best on forecast periods with M4+ earthquakes, when it possesses low scores.

This is mirrored by the second panel, which shows the difference  $\bar{S}_t^{(j)} - \bar{S}_t^{(k)}$  in the daily scores between the LM model ( $k$ ), which we employ as reference throughout the paper, and its competitors ( $j$ ), again using the Poisson scoring function. In forecast periods with M4+ earthquakes, the majority of the score differences are positive, so the LM model attains the best scores and the FCM model the worst scores for these periods. A look back at the top panel of Figure 2 provides a straightforward explanation: the LM model issues the highest expected count forecasts, whereas the FCM model issues the lowest forecasts.

To check for statistically significant differences in forecast performance, we apply the Diebold–Mariano test on the daily scores  $\bar{S}_t^{(j)}$  from (2), which operates under the null hypothesis that model  $j$  and model  $k$  perform equally well in terms of the scoring

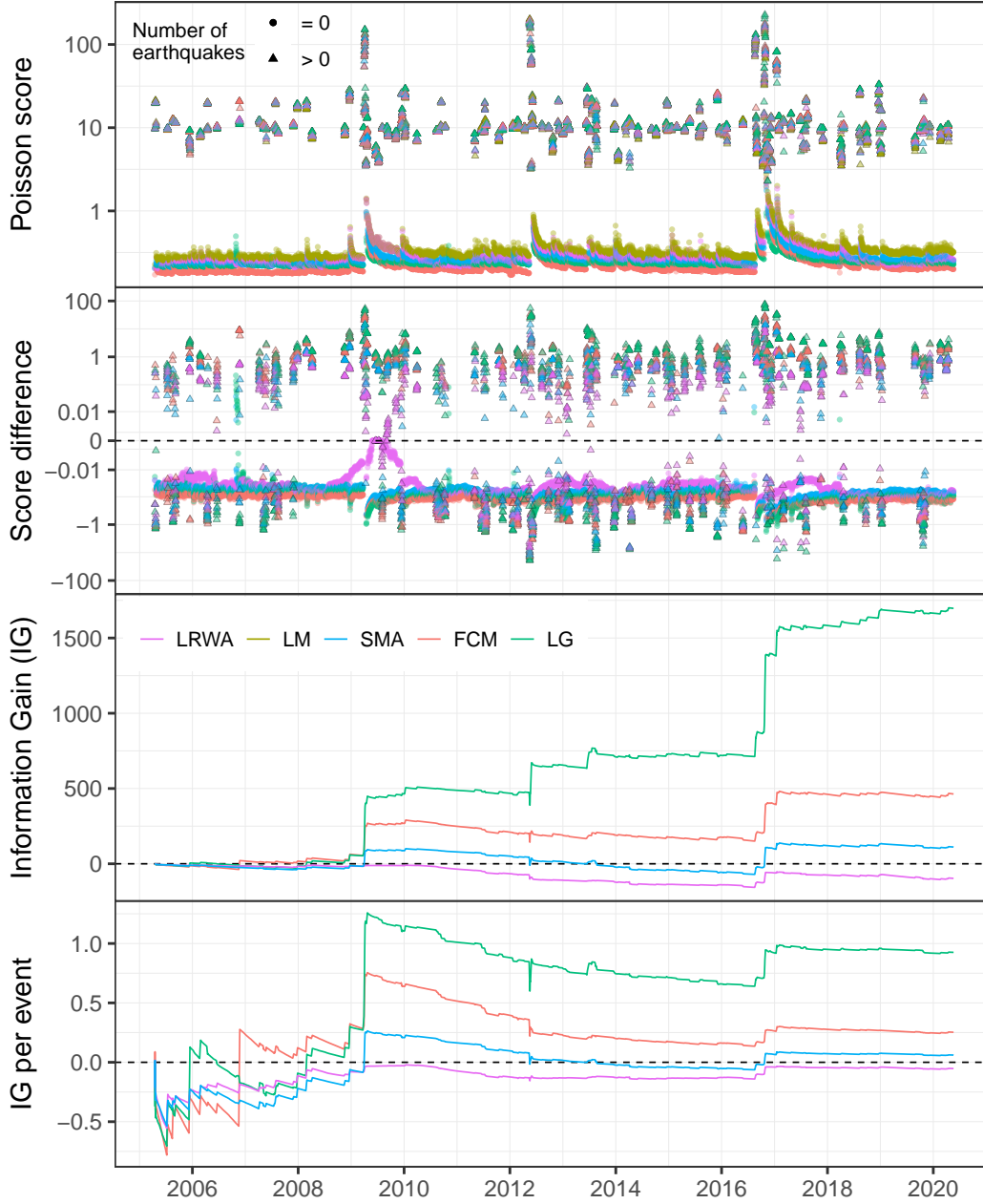


Figure 4: From top to bottom: Spatially aggregated daily Poisson score (2) for the five forecast models; Daily Poisson score difference relative to the LM model; Cumulative Poisson score difference or information gain (IG) of the LM model over the other models; Information gain per earthquake (IGPE) of the LM model over the other models. In the first two panels, two different markers are used: triangles for cells that contain one or more M4+ target earthquakes, and circles otherwise. Note the logarithmic scale in the upper two panels. All quantities are negatively oriented, i.e., the smaller the better for the color coded model. For technical details see Appendix B.1.

function  $S$ . If the null hypothesis is true, the test statistic

$$z_{(j,k)} = \sqrt{T} \frac{\bar{S}^{(j)} - \bar{S}^{(k)}}{\hat{\sigma}_{(j,k)}} \quad (12)$$

has a standard normal distribution in the limit as the number  $T$  of testing times grows larger. In (12),  $\hat{\sigma}_{(j,k)}^2$  is an estimate of the variance of the daily score differences that accounts for temporal dependencies, namely,

$$\hat{\sigma}_{(j,k)}^2 = \hat{\gamma}_{(j,k)}(0) + 2 \sum_{l=1}^L \hat{\gamma}_{(j,k)}(l) \quad (13)$$

where

$$\hat{\gamma}_{(j,k)}(l) = \frac{1}{T} \sum_{t=l+1}^T (\bar{S}_t^{(j)} - \bar{S}_t^{(k)} - \bar{d}_{(j,k)}) (\bar{S}_{t-l}^{(j)} - \bar{S}_{t-l}^{(k)} - \bar{d}_{(j,k)}) \quad \text{and} \quad \bar{d}_{(j,k)} = \bar{S}^{(j)} - \bar{S}^{(k)}.$$

The summation in the expression (13) for  $\hat{\sigma}_{(j,k)}^2$  is over the sample autocovariance  $\hat{\gamma}_{(j,k)}(l)$  of the score differences at lags  $l$  up to an integer value  $L$  after which the score differentials can be considered uncorrelated. If  $L \geq 1$  then (13) applies; if  $L = 0$  then  $\hat{\sigma}_{(j,k)}^2 = \hat{\gamma}_{(j,k)}(0)$ . For OEF-Italy, we set  $L = 6$  due to the overlap of the seven-day test periods at lags up to six days.

A positive value of  $z_{(j,k)}$  at (12) arises from a smaller average score for model  $k$ ; a negative value stems from a smaller average score for model  $j$ . From  $z_{(j,k)}$ , a one-sided  $p$  value can be derived, namely,

$$p = 1 - \Phi(z_{(j,k)}), \quad (14)$$

where  $\Phi$  is the CDF of a standard normal random variable. Under the null hypothesis of equal predictive ability in terms of the scoring function  $S$  the  $p$  value at (14) is approximately uniformly distributed. A small value of  $p$  (typically, smaller than 0.01 or 0.05) allows for the rejection of the null hypothesis in favor of the alternative hypothesis of superior predictive ability of model  $k$ ; a large value of  $p$  (typically, larger than 0.95 or 0.99) suggests superior predictive ability of model  $j$ .

Table 2 shows the results for the five forecast models. The Diebold–Mariano test rejects the null hypothesis of equal predictive ability in terms of the Poisson scoring functions for all pairs of models, except for the pairs LRWA and LM, LM and SMA, and LM and FCM. The LRWA ensemble model shows the best performance in terms of the Poisson score, with score differences that are statistically significant, except for the comparison to the LM model.

A correct test of significance generates  $p$  values that are uniform between 0 and 1 when the null hypothesis is true, and shows power by rejecting the null hypothesis when it is false. We now report on a simulation experiment that demonstrates these desirable properties for the Diebold–Mariano test. First, we consider two models for which the null

Table 2: Diebold–Mariano test of the null hypothesis of equal predictive ability in terms of the Poisson scoring function for CSEP Italy models. We show the respective total Poisson score (diagonal), the  $z$  statistic (above diagonal), and one-sided  $p$ -value (below diagonal). Columns identify model  $j$  and rows model  $k$  in the  $z$  statistic at (12).

	LRWA	LM	SMA	FCM	LG
LRWA	2.69	1.17	1.64	2.27	2.84
LM	0.12	2.71	0.60	1.56	2.45
SMA	0.05	0.27	2.73	2.46	3.05
FCM	0.01	0.06	0.01	2.80	2.83
LG	0.00	0.01	0.00	0.00	3.02

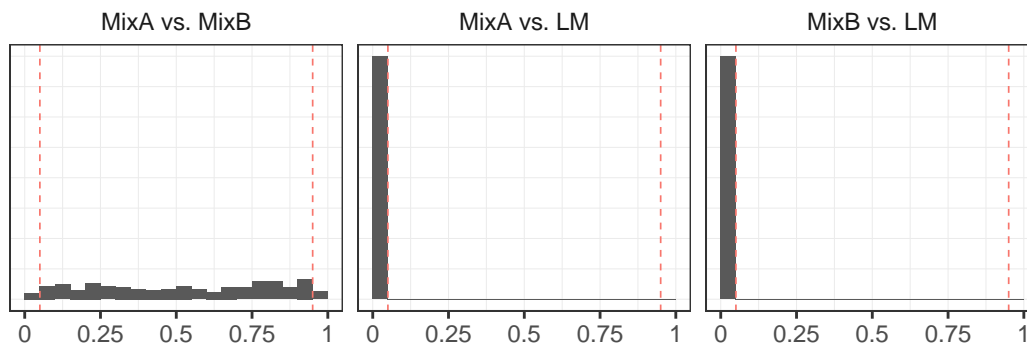


Figure 5: Histogram of  $p$  values for Diebold–Mariano tests of equal predictive ability in terms of the Poisson scoring function for (Left)  $\text{Mix}_A$  versus  $\text{Mix}_B$ ; (Middle)  $\text{Mix}_A$  versus LM; and (Right)  $\text{Mix}_B$  versus LM, based on 400 replicates.

Table 3: Predictive performance according to the total Poisson score ( $\bar{S}^{(j)}$ ), the Poisson score difference, information gain  $IG_{(j,k)}$ , and information gain per earthquake ( $IG_{(j,k)}^{\text{PE}}$ ) of the LM model ( $k$ ) relative to the model at hand ( $j$ ). The best (lowest) score in each column is highlighted in green.

	$\bar{S}^{(j)}$	$\bar{S}^{(j)} - \bar{S}^{(k)}$	$IG_{(j,k)}$	$IG_{(j,k)}^{\text{PE}}$
LM	2.71	0.000	0.000	0.000
FCM	2.80	0.084	463.572	0.253
LG	3.02	0.308	1697.038	0.925
SMA	2.73	0.020	111.393	0.061
LRWA	2.69	-0.018	-96.795	-0.053

hypothesis of equal predictive ability is true. To achieve this, we define models  $\text{Mix}_A$  and  $\text{Mix}_B$  in the setting of OEF-Italy. At any given time  $t$ ,  $\text{Mix}_A$  chooses randomly between the FCM and the LG forecast, with equal probability, whereas  $\text{Mix}_B$  uses the other forecast. By design,  $\text{Mix}_A$  and  $\text{Mix}_B$  have equal predictive ability. The histogram at left in Figure 5 shows the  $p$  values that arise from 400 replicates of Diebold–Mariano tests of  $\text{Mix}_A$  (index  $j$ ) versus  $\text{Mix}_B$  (index  $k$ ); as desired, the histogram is nearly uniform. The histograms at middle and at right in Figure 5 show the  $p$  values in the 400 tests of  $\text{Mix}_A$  versus LM, and  $\text{Mix}_B$  versus LM, respectively, which all lead to the rejection of the null hypothesis in favor of superior predictive ability of the LM model.

## 2.4 Comparison to the CSEP T-test

At this stage, let us compare to the CSEP T-test, which also aims to compare the predictive ability of two models. As proposed by Rhoades et al. (2011, Section 2.3), the CSEP T-test of equal predictive ability is based on quantities called the *information gain* ( $IG_{(j,k)}$ ) and the *information gain per earthquake* ( $IG_{(j,k)}^{\text{PE}}$ ) of model  $k$  over model  $j$ , respectively. In Appendix B.2 we prove that

$$IG_{(j,k)} = T \left( \bar{S}^{(j)} - \bar{S}^{(k)} \right) \quad \text{and} \quad IG_{(j,k)}^{\text{PE}} = \frac{T}{N_T} \left( \bar{S}^{(j)} - \bar{S}^{(k)} \right), \quad (15)$$

where  $N_T = \sum_{t=1}^T \sum_{c=1}^C y_{c,t}$ , are both multiples of the Poisson score difference  $\bar{S}^{(j)} - \bar{S}^{(k)}$ . Table 3 illustrates the relationships between the total Poisson score, the Poisson score difference, the information gain  $IG_{(j,k)}$ , and the information gain per earthquake  $IG_{(j,k)}^{\text{PE}}$  for the five forecast models, where the index  $k$  stands for the LM model, the index  $j$  for the model at hand, and where  $T = 5514$  and  $N_T = 1834$ .

These relationships demonstrate two key insights. First,  $IG_{(j,k)}$  and  $IG_{(j,k)}^{\text{PE}}$  are perfectly valid tools for comparing the predictive performance of model forecasts in the form of expected earthquake counts. Second, despite their derivation in terms of Poisson likelihoods in Rhoades et al. (2011), the use of  $IG_{(j,k)}$  and  $IG_{(j,k)}^{\text{PE}}$  does not depend on

the assumption of Poisson-distributed earthquake counts, nor does it rely on any other parametric distributions. The only assumption that needs to be made is that the model forecasts represent expected counts in the technical sense of the expectation or mean of a random variable, as pointed out previously (Brehmer et al., 2024). Importantly, these arguments support the use of  $IG_{(j,k)}$  and  $IG_{(j,k)}^{\text{PE}}$  in much broader settings than previously thought feasible.

As noted before, additional procedures and assumptions are required to make formal statistical inference. In this regard, the T-test proposed in Section 2.3 of Rhoades et al. (2011) has shortcomings. In a nutshell, the variance estimate is incorrectly specified. As a consequence, the  $p$  values generated by the T-test generally fail to be uniform under the null hypothesis of equal predictive ability. For details, we refer to Appendix B.3, where we demonstrate these issues in displays analogous to Table 2 and Figure 5. In this light, we recommend that the CSEP T-test be replaced by the Diebold–Mariano test based on spatially aggregated Poisson scores. The two approaches rank models in the very same way, but they differ in the statistical properties of the tests, and only the Diebold–Mariano test shows the desired behaviour under the null hypothesis.

### 3 Calibration, reliability, and discrimination

Up to now we have focused on comparative evaluation of the models — we have asked whether a model is better than its competitors. We now turn to the question of calibration and ask how well a model’s forecasts agree with the outcomes. Briefly, calibration is a joint property of the forecasts and the outcomes that summarizes the degree of mutual consistency. It thus addresses the question whether a forecast provides reliable information about the outcomes. This kind of testing has been originally named *consistency tests* since the first CSEP-related studies (e.g., Werner et al., 2010) and its predecessor (Schorlemmer et al., 2007); it puts the focus on formal statistical tests of the agreement between forecasts and observations given specific parametric assumptions. In other scientific fields, these types of questions have been addressed via the *calibration* concept (e.g., Gneiting et al., 2007; Gneiting and Resin, 2023). Similar to CSEP’s consistency definition, calibration refers to the statistical consistency between the forecasts and the observations. However, similar to the point process-oriented techniques proposed by Bray and Schoenberg (2013), Thorarinsdottir (2013), and Bray et al. (2014), our focus here is on calibration checks from a diagnostic perspective, where the goal is to identify, and eventually remedy, model deficiencies.

#### 3.1 Conditional calibration

Since our study deals with models that produce forecasts for the expected or mean number of earthquakes, we ask whether the forecasts are mean-calibrated, i.e., whether the forecasted means are consistent with the observed numbers of earthquakes. To state this mathematically, we follow Gneiting and Resin (2023) and conceptualize in terms of a random vector  $(X, Y)$  where  $X$  is the forecast and  $Y$  the corresponding observation.



Then the forecast  $X$  is *conditionally mean-calibrated*, or simply *calibrated*, if

$$\mathbb{E}(Y | X) = X \tag{16}$$

holds, i.e., if the conditional mean or expectation of the outcome, given any forecast value  $X = x$ , equals  $x$ . In practice, mean calibration implies, e.g., that, considering all grid cells and days on which an expected count of  $x = 0.70$  earthquakes is forecasted, the number of observed earthquakes averages to 0.70.<sup>7</sup> Hence, such a forecast is also termed *reliable*. Naturally, no real-world model can provide perfectly calibrated forecasts, thus we are more interested in how much it deviates from the ideal in (16). The problem of a model’s validation, which is a basic component of any scientific enterprise, requires further work, because it should also consider epistemic uncertainty (Marzocchi and Jordan, 2018). We intend to address this issue in future work.

### 3.2 Mean-reliability curves

In situations where the forecasts take only a few different values, it is straightforward to check for mean-calibration by pooling forecasts with a specific value and, for each of such group, comparing to the corresponding average value of the outcomes. However, mean-forecasts usually take arbitrarily different values, such that this approach is inappropriate without cumbersome and possibly subjective binning of the forecasts. The recently developed CORP (Consistent, Optimally binned, Reproducible, and PAV algorithm based) approach of Dimitriadis et al. (2021) and Gneiting and Resin (2023) addresses these issues and yields a mathematically principled, graphical assessment of mean calibration. While the initial development by Dimitriadis et al. (2021) concerned probability forecasts of binary outcomes, we follow Gneiting and Resin (2023) in considering mean-forecasts of real-valued outcomes.

Given a set of forecast–observation pairs  $(x_1, y_1), \dots, (x_n, y_n)$  the CORP approach uses nonparametric isotonic mean regression to calculate a sequence of (re) calibrated values  $\hat{x}_1, \dots, \hat{x}_n$ , respectively. The nonparametric isotonic regression approach is implemented by the classical pool adjacent violators (PAV) algorithm (Ayer et al., 1955; de Leeuw et al., 2009). As described in Algorithm 1, the PAV technique sorts the forecast–observation pairs and then partitions the index set  $\{1, \dots, n\}$  into bins  $B_{k:l} = \{k, \dots, l\}$  of consecutive integers, which are pooled in an iterative fashion, until mean-calibration is achieved. The resulting nonparametric isotonic regression curve yields a calibrated value  $\hat{x}$  for the original forecast value  $x$ . When viewed as a function of the original forecast values, and interpolated linearly in between, the calibrated values form a nondecreasing, piecewise linear curve that typically includes horizontal segments.

The calibrated value  $\hat{x}$  is an estimate of the conditional expectation  $\mathbb{E}(Y | X = x)$  and thus it should be close to  $x$  under the mean-calibration property in (16). The *mean-reliability curve* is the graph of the piecewise linear function that arises from an interpolation of the points  $(x_1, \hat{x}_1), \dots, (x_n, \hat{x}_n)$ , where we assume, for simplicity of the description, that  $x_1 \leq \dots \leq x_n$ . Horizontal segments in a mean-reliability curve

---

<sup>7</sup>In estimation problems, this type of property is commonly referred to as *unbiasedness*.

**Input:** tuples  $(x_1, y_1), \dots, (x_n, y_n)$   
**Output:** calibrated values  $\hat{x}_1, \dots, \hat{x}_n$   
rearrange indices such that  $x_1 \leq \dots \leq x_n$   
partition into bins  $B_{1:1}, \dots, B_{n:n}$  and let  $\hat{x}_i = x_i$  for  $i = 1, \dots, n$   
**while** there are bins  $B_{k:i}$  and  $B_{(i+1):l}$  such that  $\hat{x}_1 \leq \dots \leq \hat{x}_i$  and  $\hat{x}_i > \hat{x}_{i+1}$  **do**  
| merge  $B_{k:i}$  and  $B_{(i+1):l}$  into  $B_{k:l}$  and let  $\hat{x}_i = (x_k + \dots + x_l)/(l - k + 1)$  for  
|  $i = k, \dots, l$   
**end**

**Algorithm 1:** PAV algorithm based on forecast–outcome tuples  $(x_1, y_1), \dots, (x_n, y_n)$ . The rearrangement of the indices allows for a succinct description of the algorithm, which is adopted from [Gneiting and Resin \(2023, p. 3249\)](#).

then correspond to distinct forecast values  $x_i \leq \dots \leq x_j$  such that  $\hat{x}_i = \dots = \hat{x}_j$ . A perfectly calibrated forecast has a mean-reliability curve directly on the diagonal. Major deviations from the diagonal in the mean-reliability diagram indicate a lack of mean calibration and can be interpreted diagnostically.

In the spatio-temporal setting of earthquake forecasting, we have  $n = C \times T$  and the forecast–observation pairs  $(x_1, y_1), \dots, (x_n, y_n)$  correspond to the collection of tuples

$$\left( x_{c,t}^{(j)}, y_{c,t} \right)_{c=1, \dots, C; t=1, \dots, T}$$

with forecast values  $x_{c,t}^{(j)}$  from model  $j$  and corresponding counts  $y_{c,t}$  of target earthquakes. For an initial illustration, Figure 6 provides mean-reliability diagrams for the LM forecast and artificially manipulated variants thereof. As the forecast values are mostly very small, the typical linear–linear diagram is hard to interpret in this setting. Instead, we plot reliability diagrams on an empirical CDF scale on both the horizontal and the vertical axes. Specifically, we use the empirical CDF of the forecast values over all five models (LM, FCM, LG, SMA, and LRWA), all grid cells, and all test times to scale the axes. For example, a linear value of 0.20 indicates the 20th percentile in this aggregated distribution, and the tickmarks correspond to 0,  $10^{-7}$ ,  $10^{-6}$ ,  $10^{-5}$ ,  $10^{-4}$ , and the maximum 0.88 of the forecast values, respectively. The mean-reliability curve for the LM model in the left panel is rather close to the diagonal, as desired, though it remains below the diagonal, and in fact at zero, for forecast values up to about  $3.3 \cdot 10^{-6}$ . The same panel also shows the mean-reliability curve for the perfectly (re) calibrated LM forecast (LM rc), which is directly on the diagonal, as enforced by the PAV algorithm.

The middle panel in Figure 6 shows mean-reliability curves that result from underforecasting and overforecasting, respectively. Specifically, the LM  $\times 4$  forecast multiplies the expected count under the LM model by a factor of 4. This results in overforecasts, with observed earthquake counts that are substantially lower on average than the manipulated forecast value and, therefore, a mean-reliability curve that is well below the diagonal. The LM  $\times 0.25$  forecast divides the LM forecast by a factor of 4, which results in underforecasts and a mean-reliability curve mostly well above the diagonal. Finally, we consider an overconfident variant of the LM model (‘LM overconf’) that issues fore-

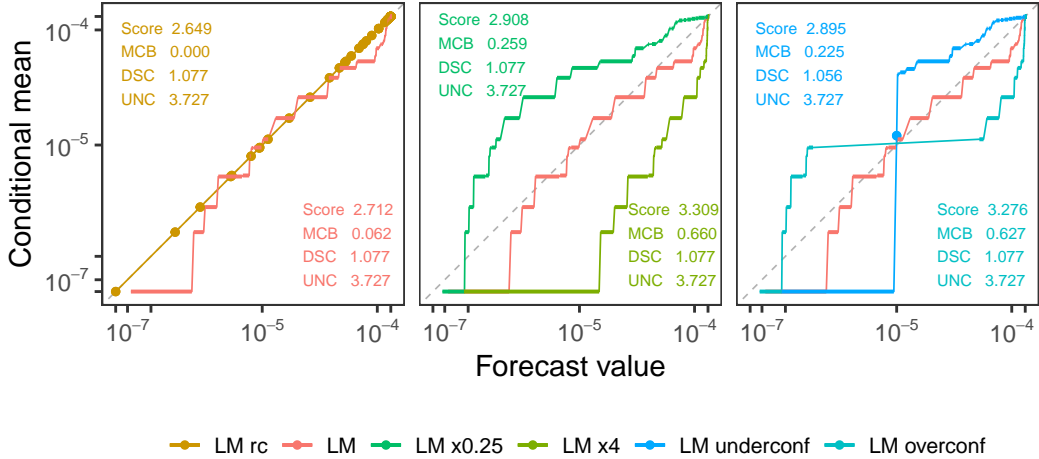


Figure 6: Mean-reliability curves for the LM forecast and artificially manipulated variants thereof as described in the text, using an empirical CDF transform aggregated over all models to scale the axes. The tickmarks correspond to non-transformed, original values of 0,  $10^{-7}$ ,  $10^{-6}$ ,  $10^{-5}$ ,  $10^{-4}$ , and 0.88, respectively. We also show the associated total Poisson score at (1) and its decomposition into miscalibration (MCB), discrimination (DSC), and uncertainty (UNC) components from (19), as described in Section 3.3.

cast values too far out in the tails, and an underconfident version (‘LM underconf’) that pushes the forecast values away from the extreme tails.<sup>8</sup> The mean-reliability curves show the characteristic S-shape for an underconfident forecast, and the typical inverse S-shape for an overconfident forecast, respectively.

Figure 7 shows reliability diagrams for the five forecast models. In practice, mean-reliability curves deviate from the diagonal even when the hypothesis of mean calibration is true, for reasons of sampling variability alone. We use *consistency bands* to address the question whether an observed deviation from the diagonal can reasonably be attributed to random (sampling) fluctuations alone, despite the forecasts being calibrated. Thus, the 90 per cent consistency bands in Figure 7 range (pointwise) from the 5th to the 95th percentile of mean-reliability curves that are sampled under the hypothesis of mean-calibration, using the method described in Appendix C. In addition to the mean-reliability curves, we show histograms for the forecast values for the model at hand, using the same empirical CDF scale based on all five models aggregated, as described above and used for the mean-reliability curves. The LM model is well calibrated as its mean-reliability curve fluctuates around the diagonal mostly within the 90 per cent consistency band that quantifies the variation of the calibration curve under the

<sup>8</sup>Specifically, the LM overconf forecast agrees with LM  $\times 0.25$  for an LM model output  $\leq 10^{-5}$  and agrees with LM  $\times 4$  for an LM model output  $> 10^{-5}$ . The LM underconf forecast agrees with LM  $\times 4$  for an LM model output  $\leq 0.25 \cdot 10^{-5}$ , agrees with LM  $\times 0.25$  for an LM model output  $\geq 4 \cdot 10^{-5}$ , and equals  $10^{-5}$  otherwise.

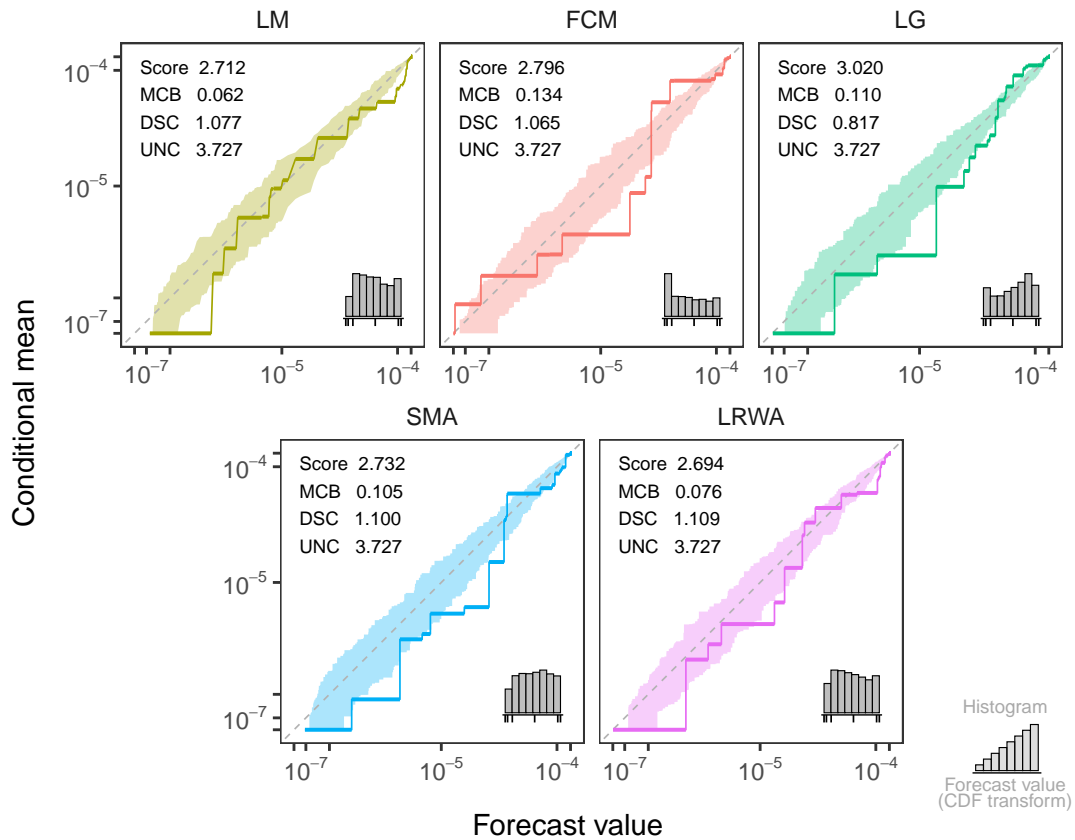


Figure 7: Mean-reliability curves as in Figure 6, but for the five OEF-Italy forecast models, along with 90 per cent consistency bands (shaded), using an empirical CDF transform aggregated over all models to scale the axes. The inset histograms depict the distribution of a model’s forecast values after this transform.

hypothesis of mean-calibration. In contrast, the calibration curves of the FCM, LG, and SMA models oftentimes leave the consistency bands. Apart from the FCM model, which frequently issues very small forecasts, as indicated by the spike at the lower range of the inset histogram, small and moderate forecast values generally tend to be too large (i.e., overforecasting) since the calibration curve is beneath the diagonal for small forecasted means, and large forecast values (on the CDF scale) tend to be too small (i.e., underforecasting), for a slight indication of underconfidence.

### 3.3 Miscalibration–discrimination (MCB–DSC) diagrams

As illustrated in Figures 6 and 7, mean-reliability curves allow for a diagnostic interpretation of a model’s performance in terms of calibration. In a related development, and also based on the CORP (re) calibration method, [Gneiting and Resin \(2023\)](#) introduce a decomposition of the average score

$$\bar{S} = \frac{1}{n} \sum_{i=1}^n S(x_i, y_i) \quad (17)$$

for a collection  $(x_1, y_1), \dots, (x_n, y_n)$  of forecast–observation pairs that allows for an interpretation in terms of (mis) calibration and discrimination ability. Specifically, let  $\hat{x}_1, \dots, \hat{x}_n$  denote the PAV (re) calibrated forecasts that correspond to  $x_1, \dots, x_n$ , respectively, and let  $\hat{x}_{\text{mg}} = \frac{1}{n} \sum_{i=1}^n y_i$  denote the overall (or marginal) mean, which serves as a simple baseline mean-forecast. Given a consistent scoring function  $S$  we let

$$\bar{S}_{\text{rc}} = \frac{1}{n} \sum_{i=1}^n S(\hat{x}_i, y_i) \quad \text{and} \quad \bar{S}_{\text{mg}} = \frac{1}{n} \sum_{i=1}^n S(\hat{x}_{\text{mg}}, y_i)$$

denote the average score of the (re) calibrated forecast and the marginal forecast, respectively. We can then define the *miscalibration* (MCB), *discrimination* (DSC), and *uncertainty* (UNC) components of the average score  $\bar{S}$  as

$$\text{MCB} = \bar{S} - \bar{S}_{\text{rc}}, \quad \text{DSC} = \bar{S}_{\text{mg}} - \bar{S}_{\text{rc}}, \quad \text{and} \quad \text{UNC} = \bar{S}_{\text{mg}} \quad (18)$$

respectively. The MCB term compares the original forecast to the calibrated one, and attains its minimal value of zero if, and only if, the original forecast is calibrated; the DSC term compares the best constant forecast to the calibrated forecast, and attains its minimal value of zero if, and only if,  $x_i = x_1$  for  $i = 1, \dots, n$  ([Gneiting and Resin, 2023](#)). In other words, the MCB reflects how unreliable a model is, whereas the DSC term reflects how well a model can sort out different scenarios (e. g., here especially background seismicity and triggered seismicity). The UNC term is independent of the issued forecast values and quantifies the variability of the outcomes. All three components are nonnegative and yield the CORP score decomposition

$$\bar{S} = \text{MCB} - \text{DSC} + \text{UNC}. \quad (19)$$

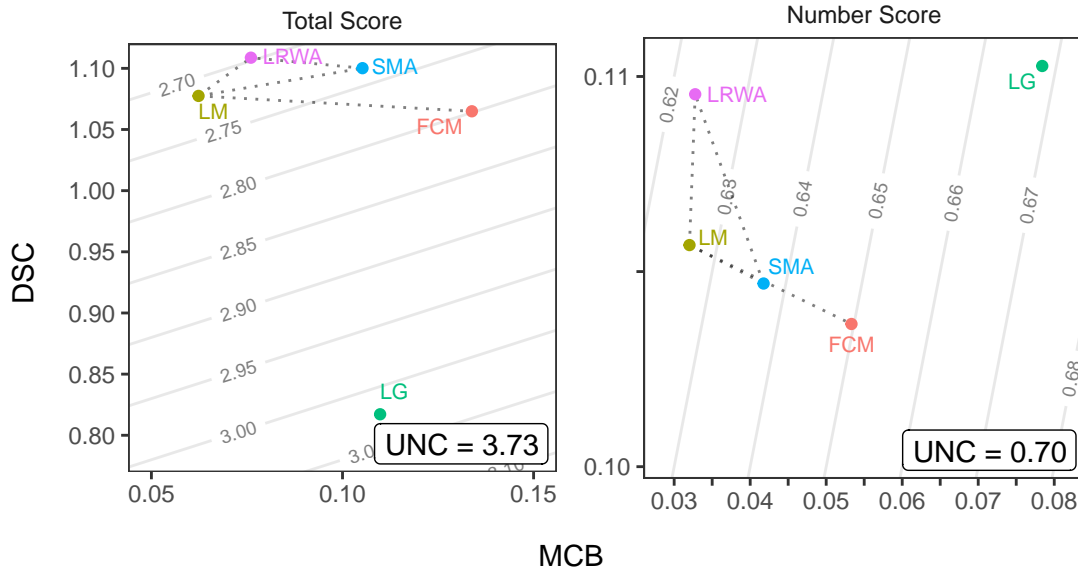


Figure 8: MCB–DSC diagram for the five forecast models under the Poisson scoring function, for (Left) the total score at (1) and (Right) the number score at (20). For the pairs of models connected by (dotted) lines, the (two-sided) Diebold–Mariano test does not reject the null hypothesis of equal predictive ability in terms of the Poisson scoring function at the 0.10 significance level.

Evidently, low MCB and high DSC terms are desirable, and a low average score  $\bar{S}$  might stem from low MCB, or high DSC, or both. Analogously, a high average score might stem from high MCB, or low DSC, or both.

For an illustration of the decomposition (19) under the Poisson scoring function on manipulated LM forecasts we return to Figure 6, where  $n = C \times T$ . We note that the (re) calibrated LM forecast shares DSC with the original LM model, but has lower (namely, zero) MCB. The LM  $\times 4$  and LM  $\times 0.25$  forecasts also share DSC with the original LM model, but have much larger MCB. These observations highlight that DSC only reflects the relative context of a model’s forecast values. The ‘LM overconf’ and ‘LM underconf’ forecasts degrade MCB and/or DSC. Similarly, Figure 7 illustrates the decomposition (19) for the five forecast models under the Poisson scoring function.

For a more succinct presentation of the CORP score decomposition at (19) we consider miscalibration–discrimination (MCB–DSC) diagrams, as introduced in related contexts by Dimitriadis et al. (2023) and Gneiting et al. (2023). An MCB–DSC diagram plots, for each model considered, DSC on the vertical axis versus MCB on the horizontal axis. In view of the relationship at (19), models with an equal average score  $\bar{S}$  are represented on parallel lines with positive slope,<sup>9</sup> and models at upper left in the diagram

<sup>9</sup>As the relationships in (15) demonstrate, these lines also indicate equal information gain, or equal information gain per earthquake.

score best, with low MCB and high DSC, whereas models at lower right score worst, with high MCB and low DSC. Models that are located (roughly) on one of the parallel lines have a similar average score but trade MCB for DSC, or vice versa. The left panel in Figure 8 shows an MCB–DSC diagram for the five forecast models from Figure 7 using the total score (1). Accordingly, the inferior performance of the LG model stems from a substantial lack of discrimination ability (evidently from Figure 4, it performs well for quiescent periods, i.e., background seismicity, but worst during the sequences in central Italy 2009 and 2016). The LRWA and LM models outperform their competitors and show pleasant balance between calibration and discrimination. The differences in the total score between the LRWA, LM, SMA, and FCM models are modest.

The right panel in Figure 8 shows an MCB–DSC diagram for spatially aggregated model forecasts, as shown in the top panel of Figure 2. Specifically, the *number score* of model  $j$ ,

$$\bar{S}_{\#}^{(j)} = \frac{1}{T} \sum_{t=1}^T \mathcal{S} \left( \sum_{c=1}^C x_{c,t}^{(j)}, \sum_{c=1}^C y_{c,t} \right), \quad (20)$$

is the average score of the spatially aggregated expected numbers of earthquakes.<sup>10</sup> In typical practice, analyses based on total scores as in (1) and analyses based on number scores as in (20) yield similar, if not identical, model rankings. Yet, we prefer total scores since comparisons of spatially aggregated forecasts in number scores ignore regional differences in predictive performance. For example, a model that overforecasts in some part of the testing region and underforecasts in another part gets penalized by the total score in (1), but if both balance each other, the model’s deficiencies may not be discernible from the number score in (20). In the spatially aggregated setting, the number of forecast cases dwindles to  $n = T$ , as opposed to  $n = C \times T$  for the total score at the grid cell level. While the rankings of the five forecast models under the total score and under the number score are identical, the LG model now lacks predominantly in terms of MCB.

As noted, forecasts in the form of expected counts allow for aggregation at any desired spatial and/or temporal level, and we encourage the development of multi-resolution evaluation approaches in the spirit of Khawaja et al. (2023).

### 3.4 Comparison to existing CSEP methodology

Our focus in this section has been on diagnostics, where the goal is to identify, and eventually remedy, model deficiencies in terms of the notions of (mis) calibration, also referred

---

<sup>10</sup>Interestingly, if there are no target earthquakes at a given time  $t$ , then the models’ contributions to the total score equal their contributions to the number score. This follows from the fact that if  $\mathcal{S}$  is the Poisson scoring function at (9) then

$$\bar{S}_t^{(j)} = \sum_{c=1}^C \mathcal{S}(x_{c,t}^{(j)}, y_{c,t}) = \mathcal{S} \left( \sum_{c=1}^C x_{c,t}^{(j)}, \sum_{c=1}^C y_{c,t} \right) + \sum_{c=1}^C \mathcal{S} \left( \frac{x_{c,t}^{(j)}}{\sum_{b=1}^C x_{b,t}^{(j)}}, y_{c,t} \right) - 1.$$

The middle term on the right-hand side reduces to the constant 1 if  $y_{c,t} = 0$  for  $c = 1, \dots, C$ , which proves the claim.

to as reliability, and discrimination ability. In contrast, extant CSEP methodology for model evaluation has put the focus on formal statistical tests of agreement between forecasts and outcomes, frequently under the label of *earthquake likelihood model testing* (Kagan and Jackson, 1995; Schorlemmer et al., 2007). For example, the CSEP L-test, CL-test, and N-test operate under the (questionable) joint hypothesis that the modeled expected cell counts are correct, and that each observed count has a Poisson distribution. A model then might fail the test when either one or both of the hypotheses are false. In particular, this happens when the expected cell counts are perfectly correct, but the observed counts do not come from the Poisson distribution. Conversely, while a passed test expresses the fact that there is no evidence against either of the hypotheses, a model might pass the test, and yet be inferior to competitors that fail the test. Thus, the outcomes of these tests may be misleading, except for cases where the model issues full-distribution forecasts that are explicitly Poisson distributions.

The Poisson assumption was avoided by Savran et al. (2020), who tested full-distribution (i.e., catalog-based) earthquake forecasts with nonparametric analogs to the grid-based CSEP tests (N-, M-, L-, and S-test). These tests were implemented in (py)CSEP (Savran et al., 2022), but they only address consistency/calibration of full-distribution forecasts, not comparative evaluations. The tools proposed here are also nonparametric and do not rely on a Poisson assumption. They are straightforward to implement and, in addition to model ranking via scoring functions, they can be used diagnostically, via mean-reliability curves and MCB-DSC diagrams, to identify, and eventually remedy, model deficiencies. In addition, the proposed methods facilitate comparing also full-distribution forecasts.

Worthy of note, as for the current CSEP testing implementation, both calibration and consistency tests do not account for the so-called epistemic uncertainty, considering only one model or the (weighted) mean of a set of models. The consequences of that have been discussed in depth by Marzocchi and Jordan (2014). Here we just mention that a proper model validation can be made only considering such an uncertainty. Hence, model consistency and calibration have mostly an heuristic value that tells us how much and how the observations deviate from the forecasts.

## 4 Conclusion

In this study we considered short-term earthquake forecasting models for the Italian CSEP testing region and evaluated their forecasts (in the form of expected earthquake counts) with consistent scoring functions, mean-reliability diagrams, and miscalibration–discrimination (MCB–DSC) diagrams. We illustrated that evaluation methods based on scoring functions offer a comprehensive assessment of the models. They yield a broader perspective on the existing CSEP testing framework and provide a valuable tool box for earthquake model assessment. Specifically, we make the following recommendations.

- There are many consistent scoring functions for forecasts in the format of expected counts, with the Poisson score playing a distinguished role in low probability environments. Use Murphy diagrams to consider all consistent scoring functions



simultaneously; the area under a logarithmic Murphy curve equals the average Poisson score.

- Retain the established practice of binary model comparisons via the information gain per earthquake ( $\text{IG}^{\text{PE}}$ : Harte and Vere-Jones, 2005; Rhoades et al., 2011) measure. The  $\text{IG}^{\text{PE}}$  measure equals (up to a factor) the difference in the average Poisson score (Eq. 15) and is much broader applicable than previously thought, as its use does not depend on any parametric assumptions.
- If formal inference is the goal, replace the CSEP T-test by the Diebold–Mariano test based on spatially aggregated scores, which accounts for spatio-temporal dependencies.
- Use mean-reliability curves as a diagnostic tool to assess calibration.
- An average score  $\bar{S}$  can be decomposed into MCB, DSC, and UNC components. Compare and investigate them for multiple models in MCB–DSC diagrams.

We are confident that these tools will help pave the way to improvements in the evaluation, selection, and development of earthquake forecasting models.

While thus far we have considered overall assessments of a model’s predictive performance, we might also ask in which areas of the testing region one can find remarkable differences in forecast performance. To do so we can study performance via average scores for each of the 8993 grid cells in OEF-Italy. Specifically, we consider the average score difference between model  $j$  and model  $k$  in grid cell  $c$ , given by

$$\Delta_c^{(j,k)} = \frac{1}{T} \sum_{t=1}^T \left( S(x_{c,t}^{(j)}, y_{c,t}) - S(x_{c,t}^{(k)}, y_{c,t}) \right), \quad (21)$$

where  $S$  is the Poisson scoring function. We again let  $k$  stand for the LM model. Positive values of  $\Delta_c^{(j,k)}$  indicate that the LM model produces superior forecasts in grid cell  $c$ .

Figure 9 plots  $\Delta_c^{(j,k)}$ , i.e., the average score difference between the LM model and model  $j$  in grid cell  $c$  for the four competitor models. In line with our previous analysis, the LM model exhibits superior forecast performance in most grid cells with observed M4+ earthquakes. While the FCM model receives lower scores than the LM model in regions with less seismicity, the LG model performs worse than the LM model in those. We emphasize that these results are to be interpreted diagnostically, with formal statistical inference being challenging in spatial settings due to massive dependencies and issues of multiple testing (Zhang et al., 2015; Wilks, 2016).

It is important to stress that our results hold only in terms of mean-forecasts. In particular, we do not claim that the LRWA and LM models are superior in all facets. The results indicate that they are slightly better at producing mean-forecasts for the number of earthquakes. A key reason for this is that the forecasts of the LM model are well-calibrated and overall higher than the forecasts of its competitors. Hence, the LM model is not as severely underforecasting as the LG and FCM models on days when (many) earthquakes happen.

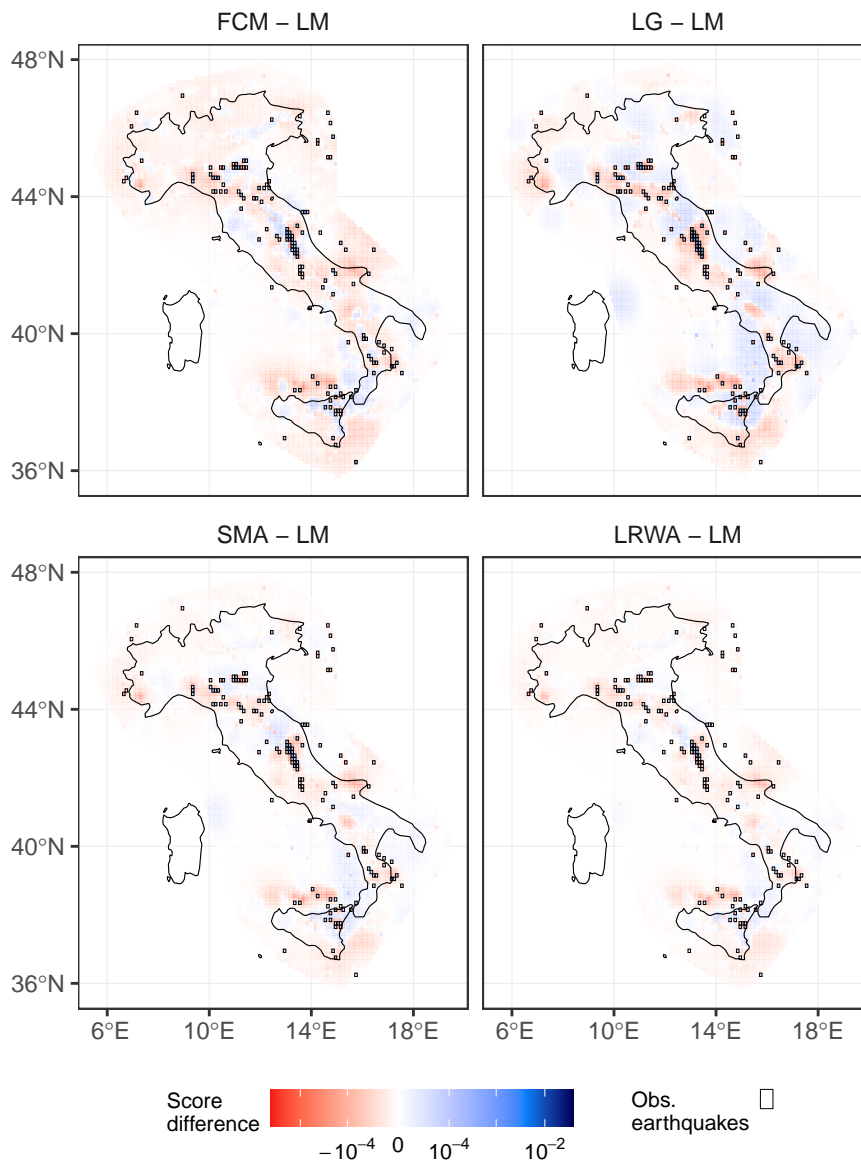


Figure 9: Average score difference (21) under the Poisson scoring function between the LM (index  $k$ ) and the CSEP Italy model at hand (index  $j$ ). Positive differences (blue color) indicate that the LM model has superior forecast performance; negative differences (red color) indicate inferior performance.

As emphasized by [Nandan et al. \(2019\)](#) it would be best if these forecasts specified the full distribution of earthquake counts, as this provides most information on the likely implications of different actions. Yet, full-distribution forecasts may not be available due to their complexity, reporting traditions, ease of forecast communication, or the need for aggregation. However, full-distribution forecasts can be supplied in the form of a collection of synthetic catalogs (also called stochastic event sets) of future earthquakes.<sup>11</sup> Importantly, if collections of synthetic catalogs are interpreted as full-distribution forecasts, we can deduce mutually consistent full (empirical) distribution forecasts at any desired level of spatial and/or temporal aggregation. The evaluation methods proposed in this paper also apply to full-distribution forecasts, by converting them to the implied mean-forecasts, as implemented here, which does not require smoothing nor parametric assumptions.

## Data Availability

The tables and figures were produced with R ([R Core Team, 2024](#)). Code for reproduction is available on [https://github.com/jbrehmer42/Earthquakes\\_Italy](https://github.com/jbrehmer42/Earthquakes_Italy). Data are available from Marcus Herrmann ([marcus.herrmann@unina.it](mailto:marcus.herrmann@unina.it)) upon request.

## Acknowledgments

Jonas Brehmer, Tilmann Gneiting, and Kristof Kraus are grateful for support by the Klaus Tschira Foundation. Marcus Herrmann and Warner Marzocchi were supported by the ‘Multi-Risk sciEnce for resilienT commUNITies undeR a changiNg climate’ (RETURN) project, funded by the European Union’s NextGenerationEU and the Italian Ministry of University and Research (MUR) under the National Recovery and Resilience Plan (PNRR; Code PE0000005). We thank Johannes Bracher, Alexander Jordan, and Johannes Resin for helpful discussions and remarks.

## References

- Ayer, M., Brunk, H. D., Ewing, G. M., Reid, W. T. and Silverman, E. (1955). An empirical distribution function for sampling with incomplete information. *Annals of Mathematical Statistics*, 26, 641–647. URL <https://www.jstor.org/stable/2236377>.
- Bayliss, K., Naylor, M., Illian, J. and Main, I. G. (2020). Data-driven optimization of seismicity models using diverse data sets: Generation, evaluation, and ranking using Inlabru. *Journal of Geophysical Research: Solid Earth*, 125, e2020JB020226. URL <https://agupubs.onlinelibrary.wiley.com/doi/10.1029/2020JB020226>.

---

<sup>11</sup>In their experiments, [Nandan et al. \(2019\)](#) use a collection of five million synthetic catalogs.

- Bray, A. and Schoenberg, F. P. (2013). Assessment of point process models for earthquake forecasting. *Statistical Science*, 28, 510–520. URL <https://doi.org/10.1214/13-STS440>.
- Bray, A., Wong, K., Barr, C. D. and Schoenberg, F. P. (2014). Voronoi residual analysis of spatial point process models with applications to California earthquake forecasts. *Annals of Applied Statistics*, 8, 2247–2267. URL <https://doi.org/10.1214/14-AOAS767>.
- Brehmer, J. R., Gneiting, T., Herrmann, M., Marzocchi, W., Schlather, M. and Storkorb, K. (2024). Using scoring functions to evaluate point process forecasts. *Annals of the Institute of Statistical Mathematics*, 76, 47–71. URL <https://doi.org/10.1007/s10463-023-00875-5>.
- Cattania, C., Werner, M. J., Marzocchi, W., Hainzl, S., Rhoades, D., Gerstenberger, M., Liukis, M., Savran, W., Christophersen, A., Helmstetter, A., Jimenez, A., Steacy, S. and Jordan, T. H. (2018). The forecasting skill of physics-based seismicity models during the 2010–2012 Canterbury, New Zealand, earthquake sequence. *Seismological Research Letters*, 89, 1238–1250. URL <https://doi.org/10.1785/0220180033>.
- Czado, C., Gneiting, T. and Held, L. (2009). Predictive model assessment for count data. *Biometrics*, 65, 1254–1261. URL <https://doi.org/10.1111/j.1541-0420.2009.01191.x>.
- Dahm, T. and Hainzl, S. (2022). A Coulomb stress response model for time-dependent earthquake forecasts. *Journal of Geophysical Research: Solid Earth*, 127, e2022JB024443. URL <https://doi.org/10.1029/2022JB024443>.
- de Leeuw, J., Hornik, K. and Mair, P. (2009). Isotone optimization in R: Pool-Adjacent-Violators Algorithm (PAVA) and active set methods. *Journal of Statistical Software*, 32, 1–24. URL <https://www.jstatsoft.org/index.php/jss/article/view/v032i05/>.
- Diebold, F. X. and Mariano, R. S. (1995). Comparing predictive accuracy. *Journal of Business & Economic Statistics*, 13, 253–263. URL <https://doi.org/10.1198/073500102753410444>.
- Dimitriadis, T., Gneiting, T., Jordan, A. and Vogel, P. (2023). Evaluating probabilistic classifiers: The triptych. *International Journal of Forecasting*. URL <https://doi.org/10.1016/j.ijforecast.2023.09.007>.
- Dimitriadis, T., Gneiting, T. and Jordan, A. I. (2021). Stable reliability diagrams for probabilistic classifiers. *Proceedings of the National Academy of Sciences of the United States of America*, 118, e2016191118. URL <https://doi.org/10.1073/pnas.2016191118>.

- Ehm, W., Gneiting, T., Jordan, A. and Krüger, F. (2016). Of quantiles and expectiles: Consistent scoring functions, Choquet representations and forecast rankings. *Journal of the Royal Statistical Society. Series B. Statistical Methodology*, 78, 505–562. URL <https://doi.org/10.1111/rssb.12154>.
- Falcone, G., Console, R. and Murru, M. (2010). Short-term and long-term earthquake occurrence models for Italy: ETES, ERS and LTST. *Annals of Geophysics*, 53, 41–50. URL <https://doi.org/10.4401/ag-4760>.
- Gerstenberger, M. C., Wiemer, S., Jones, L. M. and Reasenber, P. A. (2005). Real-time forecasts of tomorrow’s earthquakes in California. *Nature*, 435, 328–331. URL <https://doi.org/10.1038/nature03622>.
- Gneiting, T. (2011). Making and evaluating point forecasts. *Journal of the American Statistical Association*, 106, 746–762. URL <https://doi.org/10.1198/jasa.2011.r10138>.
- Gneiting, T., Balabdaoui, F. and Raftery, A. E. (2007). Probabilistic forecasts, calibration and sharpness. *Journal of the Royal Statistical Society Series B: Statistical Methodology*, 69, 243–268. URL <https://doi.org/10.1111/j.1467-9868.2007.00587.x>.
- Gneiting, T. and Katzfuss, M. (2014). Probabilistic forecasting. *Annual Review of Statistics and Its Application*, 1, 125–151. URL <https://www.annualreviews.org/doi/abs/10.1146/annurev-statistics-062713-085831>.
- Gneiting, T. and Raftery, A. E. (2007). Strictly proper scoring rules, prediction, and estimation. *Journal of the American Statistical Association*, 102, 359–378. URL <https://doi.org/10.1198/016214506000001437>.
- Gneiting, T. and Resin, J. (2023). Regression diagnostics meets forecast evaluation: Conditional calibration, reliability diagrams, and coefficient of determination. *Electronic Journal of Statistics*, 17, 3226–3286. URL <https://doi.org/10.1214/23-EJS2180>.
- Gneiting, T., Wolfram, D., Resin, J., Kraus, K., Bracher, J., Dimitriadis, T., Hagenmeyer, V., Jordan, A. I., Lerch, S., Phipps, K. and Schienle, M. (2023). Model diagnostics and forecast evaluation for quantiles. *Annual Review of Statistics and Its Application*, 10, 597–621. URL <https://doi.org/10.1146/annurev-statistics-032921-020240>.
- Harte, D. and Vere-Jones, D. (2005). The entropy score and its uses in earthquake forecasting. *Pure and Applied Geophysics*, 162, 1229–1253. URL <https://doi.org/10.1007/s00024-004-2667-2>.
- Herrmann, M. and Marzocchi, W. (2023). Maximizing the forecasting skill of an ensemble model. *Geophysical Journal International*, 234, 73–84. URL <https://doi.org/10.1093/gji/ggad020>.

- Holzmann, H. and Eulert, M. (2014). The role of the information set for forecasting — with applications to risk management. *Annals of Applied Statistics*, 8, 595–621. URL <https://www.jstor.org/stable/24521747>.
- Jordan, T. H., Chen, Y.-T., Gasparini, P., Madariaga, R., Main, I., Marzocchi, W., Papadopoulos, G., Sobolev, G., Yamaoka, K. and Zschau, J. (2011). Operational earthquake forecasting. State of knowledge and guidelines for utilization. *Annals of Geophysics*, 54, 316–391. URL <https://doi.org/10.4401/ag-5350>.
- Kagan, Y. Y. and Jackson, D. D. (1995). New seismic gap hypothesis: Five years after. *Journal of Geophysical Research: Solid Earth*, 100, 3943–3959. URL <https://agupubs.onlinelibrary.wiley.com/doi/abs/10.1029/94JB03014>.
- Khawaja, A. M., Hainzl, S., Schorlemmer, D., Iturrieta, P., Bayona, J. A., Savran, W. H., Werner, M. and Marzocchi, W. (2023). Statistical power of spatial earthquake forecast tests. *Geophysical Journal International*, 233, 2053–2066. URL <https://doi.org/10.1093/gji/ggad030>.
- Kolassa, S. (2016). Evaluating predictive count data distributions in retail sales forecasting. *International Journal of Forecasting*, 32, 788–803. URL <https://doi.org/10.1016/j.ijforecast.2015.12.004>.
- Lolli, B. and Gasperini, P. (2003). Aftershocks hazard in Italy. Part I: Estimation of time-magnitude distribution model parameters and computation of probabilities of occurrence. *Journal of Seismology*, 7, 235–257. URL <http://link.springer.com/10.1023/A:1023588007122>.
- Lombardi, A. M. and Marzocchi, W. (2010). The ETAS model for daily forecasting of Italian seismicity in the CSEP experiment. *Annals of Geophysics*, 53, 155–164. URL <https://doi.org/10.4401/ag-4848>.
- Mancini, S., Segou, M., Werner, M. J. and Cattania, C. (2019). Improving physics-based aftershock forecasts during the 2016–2017 Central Italy earthquake cascade. *Journal of Geophysical Research: Solid Earth*, 124, 8626–8643. URL <https://onlinelibrary.wiley.com/doi/10.1029/2019JB017874>.
- Marzocchi, W. and Jordan, T. H. (2014). Testing for ontological errors in probabilistic forecasting models of natural systems. *Proceedings of the National Academy of Sciences*, 111, 11973–11978. URL <https://doi.org/10.1073/pnas.1410183111>.
- Marzocchi, W. and Jordan, T. H. (2018). Experimental concepts for testing probabilistic earthquake forecasting and seismic hazard models. *Geophysical Journal International*, 215, 780–798. URL <https://doi.org/10.1093/gji/ggy276>.
- Marzocchi, W., Lombardi, A. M. and Casarotti, E. (2014). The establishment of an operational earthquake forecasting system in Italy. *Seismological Research Letters*, 85, 961–969. URL <https://doi.org/10.1785/0220130219>.

- Nandan, S., Ouillon, G., Sornette, D. and Wiemer, S. (2019). Forecasting the full distribution of earthquake numbers is fair, robust, and better. *Seismological Research Letters*, 90, 1650–1659. URL <https://doi.org/10.1029/2022JB024380>.
- Patton, A. J. (2011). Volatility forecast comparison using imperfect volatility proxies. *Journal of Econometrics*, 160, 246–256. URL <https://www.sciencedirect.com/science/article/pii/S030440761000076X>.
- R Core Team (2024). *R: A language and environment for statistical computing*. R Foundation for Statistical Computing, Vienna, Austria. URL <https://www.R-project.org/>.
- Rhoades, D., Schorlemmer, D., Gerstenberger, M., Christophersen, A., Zechar, J. D. and Imoto, M. (2011). Efficient testing of earthquake forecasting models. *Acta Geophysica*, 59, 728–747. URL <https://doi.org/10.2478/s11600-011-0013-5>.
- Savage, L. J. (1971). Elicitation of personal probabilities and expectations. *Journal of the American Statistical Association*, 66, 783–801. URL <https://doi.org/10.2307/2284229>.
- Savran, W. H., Bayona, J. A., Iturrieta, P., Asim, K. M., Bao, H., Bayliss, K., Herrmann, M., Schorlemmer, D., Maechling, P. J. and Werner, M. J. (2022). pycsep: a python toolkit for earthquake forecast developers. *Seismological Society of America*, 93, 2858–2870. URL <https://doi.org/10.1785/0220220033>.
- Savran, W. H., Werner, M. J., Marzocchi, W., Rhoades, D. A., Jackson, D. D., Milner, K., Field, E. and Michael, A. (2020). Pseudoprospective evaluation of UCERF3-ETAS forecasts during the 2019 Ridgecrest sequence. *Bulletin of the Seismological Society of America*, 110, 1799–1817. URL <https://doi.org/10.1785/0120200026>.
- Schorlemmer, D., Gerstenberger, M., Wiemer, S. and Jackson, D. (2007). Earthquake likelihood model testing. *Seismological Research Letters*, 78, 17–29. URL <https://doi.org/10.1785/gssrl.78.1.17>.
- Schorlemmer, D., Werner, M. J., Marzocchi, W., Jordan, T. H., Ogata, Y., Jackson, D. D., Mak, S., Rhoades, D. A., Gerstenberger, M. C., Hirata, N., Liukis, M., Maechling, P. J., Strader, A., Taroni, M., Wiemer, S., Zechar, J. D. and Zhuang, J. (2018). The Collaboratory for the Study of Earthquake Predictability: Achievements and priorities. *Seismological Research Letters*, 89, 1305–1313. URL <https://doi.org/10.1785/0220180053>.
- Serafini, F., Naylor, M., Lindgren, F., Werner, M. J. and Main, I. (2022). Ranking earthquake forecasts using proper scoring rules: Binary events in a low probability environment. *Geophysical Journal International*, 230, 1419–1440. URL <https://doi.org/10.1093/gji/ggac124>.

- Sharma, S., Hainzl, S., Zöeller, G. and Holschneider, M. (2020). Is Coulomb stress the best choice for aftershock forecasting? *Journal of Geophysical Research: Solid Earth*, 125, e2020JB019553. URL <https://onlinelibrary.wiley.com/doi/10.1029/2020JB019553>.
- Spassiani, I., Falcone, G., Murru, M. and Marzocchi, W. (2023). Operational earthquake forecasting in Italy: Validation after 10 yr of operativity. *Geophysical Journal International*, 234, 2501–2518. URL <https://doi.org/10.1093/gji/ggad256>.
- Taggart, R. (2022). Evaluation of point forecasts for extreme events using consistent scoring functions. *Quarterly Journal of the Royal Meteorological Society*, 148, 306–320. URL <https://doi.org/10.1002/qj.4206>.
- Taroni, M., Marzocchi, W., Schorlemmer, D., Werner, M. J., Wiemer, S., Zechar, J. D., Heiniger, L. and Euchner, F. (2018). Prospective CSEP evaluation of 1-day, 3-month, and 5-yr earthquake forecasts for Italy. *Seismological Research Letters*, 89, 1251–1261. URL <https://doi.org/10.1785/0220180031>.
- Thorarinsdottir, T. L. (2013). Calibration diagnostics for point process models via the probability integral transform. *Stat*, 2, 150–158. URL <https://doi.org/10.1002/sta4.25>.
- Werner, M. J., Zechar, J. D., Marzocchi, W., Wiemer, S. and the CSEP-Italy Working Group (2010). Retrospective evaluation of the five-year and ten-year CSEP-Italy earthquake forecasts. *Annals of Geophysics*, 53, 11–30. URL <http://www.annalsofgeophysics.eu/index.php/annals/article/view/4840>.
- Wilks, D. (2016). “The stippling shows statistically significant grid points”: How research results are routinely overstated and overinterpreted, and what to do about it. *Bulletin of the American Meteorological Society*, 97, 2263–2273. URL <https://doi.org/10.1175/BAMS-D-15-00267.1>.
- Woessner, J., Christophersen, A., Zechar, J. D. and Monelli, D. (2010). Building self-consistent, short-term earthquake probability (STEP) models: Improved strategies and calibration procedures. *Annals of Geophysics*, 53, 141–154. URL <https://doi.org/10.4401/ag-4812>.
- Zhang, L., Mai, P. M., Thingbaijam, K. K., Razafindrakoto, H. N. and Genton, M. G. (2015). Analysing earthquake slip models with the spatial prediction comparison test. *Geophysical Journal International*, 200, 185–198. URL <https://doi.org/10.1093/gji/ggv088>.



## Appendices

### A Consistent scoring functions

#### A.1 Technical details for the Bregman representation

Consider the Bregman representation (7), namely,

$$S(x, y) = \phi(y) - \phi(x) - \phi'(x)(y - x),$$

for a scoring function that is consistent for the mean-functional. For simplicity we ignore the function  $h(y)$ , and we recall that  $\phi$  is a convex function with subgradient  $\phi'$ . Regarding our setting of count data, where the mean-forecast  $x \geq 0$  is a nonnegative number, whereas the outcome  $y \in \{0, 1, \dots\}$  is a nonnegative integer, we distinguish three cases for this representation.

In case I the convex function  $\phi$  is continuous and differentiable on the nonnegative halfaxis with  $\phi(0)$  and  $\phi'(0)$  being real numbers. A key example is  $\phi(x) = x^b$  for  $b > 1$ . Then the score  $S(x, y)$  is well-defined and finite for all  $x \geq 0$  and  $y \in \{0, 1, \dots\}$ .

In case II the convex function  $\phi$  is defined on the strictly positive halfaxis with  $\phi(0) = \lim_{x \downarrow 0} \phi(x)$  being finite, but  $\phi'(0) = \lim_{x \downarrow 0} \phi'(x) = -\infty$ . A key example is  $\phi(x) = -x^b$  for  $0 < b < 1$ . Then the score  $S(x, y)$  is well-defined and finite for  $x > 0$  and  $y \in \{0, 1, \dots\}$ . To allow for the mean-forecast  $x = 0$ , we define  $S(0, 0) = 0$  and  $S(0, y) = +\infty$  for  $y \in \{1, 2, \dots\}$ , which retains consistency.

In case III the convex function  $\phi$  is defined on the strictly positive halfaxis with  $\phi(0) = \lim_{x \downarrow 0} \phi(x) = +\infty$  and  $\phi'(0) = \lim_{x \downarrow 0} \phi'(x) = -\infty$ . A key example is  $\phi(x) = x^b$  for  $b < 0$ . Then the score  $S(x, y)$  is well-defined and finite for  $x > 0$  and  $y \in \{1, 2, \dots\}$ , but there is no obvious extension that maintains consistency.

#### A.2 Extended Patton family of consistent scoring functions

The original *Patton family* of consistent scoring functions for an expected value (Patton, 2011) is parameterized in terms of a real-valued index  $b$  and defined via

$$S_b(x, y) = \begin{cases} \frac{y^b - x^b}{b(b-1)} - \frac{x^{b-1}}{b-1}(y-x), & b \notin \{0, 1\}, \\ \frac{y}{x} - \log \frac{y}{x} - 1, & b = 0, \\ y \log \frac{y}{x} - (y-x), & b = 1, \end{cases} \quad (\text{A1})$$

for an expected value  $x > 0$  and an outcome  $y > 0$ . The members  $S_b$  of the Patton family are strictly consistent scoring functions for an expected value, as they are of the

form (7) with the strictly convex function

$$\phi_b(x) = \begin{cases} \frac{x^b}{b(b-1)}, & b \notin \{0, 1\}, \\ -\log x, & b = 0, \\ x \log x, & b = 1, \end{cases} \quad (\text{A2})$$

and a certain choice of  $h(y)$ . The Patton family nests both the Poisson scoring function ( $b = 1$ ) at (9) and the quadratic scoring function ( $b = 2$ ) at (8), up to a constant factor and terms that only depend on  $y$ . However, the specific choice of  $h(y)$  yields expressions for  $S_b(x, y)$  that can be undefined when  $x = 0$  or  $y = 0$ , and so the Patton functions need to be modified to evaluate forecasts of earthquake counts.

To accommodate count data, while retaining the nesting property, we define the *extended Patton family* via

$$S_b^0(x, y) = S_b(x, y) - S_b(1, y) + \frac{1}{2}y^b - \frac{b}{2}y + \frac{3-b}{2} \quad (\text{A3})$$

for  $x > 0$  and  $y > 0$ . The members  $S_b^0$  of the extended Patton family are still strictly consistent, since  $S_b^0(x, y)$  agrees with  $S_b(x, y)$  up to terms that depend on  $y$  only, and thus they are of the form (7) with the same choice of  $\phi_b$ .

To extend  $S_b^0(x, y)$  to  $x \geq 0$  and  $y \in \{0, 1, \dots\}$  we proceed as discussed in Appendix A.1. If  $b > 1$  we are in case I and extend by continuity. If  $0 < b \leq 1$  we are in case II and extend by setting  $S_b^0(0, 0) = 0$  and  $S_b^0(0, y) = +\infty$  for  $y \in \{1, 2, \dots\}$ . If  $b \leq 0$  we are in case III, when there is no obvious extension. The expression in (A3) yields  $S_b^0(x, y) = x - y \log x$  for  $x > 0$  and  $y \in \{0, 1, \dots\}$  when  $b = 1$ , and  $S_b^0(x, y) = \frac{1}{2}(y - x)^2$  for  $x \geq 0$  and  $y \in \{0, 1, \dots\}$  when  $b = 2$ , and thus the extended Patton family nests both the Poisson scoring function and ( $\frac{1}{2}$  times) the quadratic scoring function.

## B Further technical details and results for Section 2

In this appendix, we provide further technical details and supplementary results for Section 2. Throughout, the scoring function  $S$  is the Poisson scoring function at (9). Whenever feasible, we present formulas in the generic spatio-temporal setting of earthquake forecasts, where there are  $C$  grid cells and  $T$  regularly spaced test times, with earthquake count  $y_{c,t}$  in grid cell  $c \in \{1, \dots, C\}$  at time  $t \in \{1, \dots, T\}$ . In the specific case of the OEF-Italy there are  $C = 8993$  grid cells and  $T = 5514$  test times.

### B.1 Quantities in Figure 4 panels

We give technical details for the quantities displayed in the four panels of Figure 4. To this end, suppose that model  $j$  issues forecasts in the form of expected cell counts  $x_{c,t}^{(j)}$ . As defined at (2), the spatially aggregated score of model  $j$  at time  $t$  is

$$\bar{S}_t^{(j)} = \sum_{c=1}^C S\left(x_{c,t}^{(j)}, y_{c,t}\right), \quad (\text{B1})$$

which is the quantity plotted against time  $t$  in the first (top) panel in Figure 4, where the index  $j$  stands for the LM, FCM, LG, SMA, and LRWA model, respectively. The second panel in Figure 4 shows the daily score difference

$$d_t^{(j,k)} = \bar{S}_t^{(j)} - \bar{S}_t^{(k)}, \quad (\text{B2})$$

where the index  $j$  stands for the FCM, LG, SMA, and LRWA model, and the index  $k$  for the LM model.

Not surprisingly, plots of daily Poisson scores or daily Poisson score difference are highly irregular. To obtain smoother curves, one can plot the cumulative score difference

$$D_t^{(j,k)} = \sum_{u=1}^t d_u^{(j,k)} \quad (\text{B3})$$

against time  $t$ , as in Figure 2 of [Taroni et al. \(2018\)](#) and in the third panel of our Figure 4. Alternatively, Figures 5, 6, and C2 of [Herrmann and Marzocchi \(2023\)](#) and the fourth panel of our Figure 4 plot the normalized quantity

$$D_t^{(j,k)} / N_t, \quad (\text{B4})$$

where

$$N_t = \sum_{u=1}^t \sum_{c=1}^C y_{c,u} \quad (\text{B5})$$

is the cumulative count of earthquakes over the test region and test times  $u \in \{1, \dots, t\}$ . We note that the quantities (B1) to (B4), which are displayed in the four rows of Figure 4, are all negatively oriented, i.e., the smaller the better.

## B.2 Total Poisson score, information gain, and information gain per earthquake in spatio-temporal settings

Let us recall from (1) that the total score of model  $j$  is

$$\bar{S}^{(j)} = \frac{1}{T} \sum_{t=1}^T \bar{S}_t^{(j)},$$

where  $\bar{S}_t^{(j)}$  is the spatially aggregated score for model  $j$  on day  $t$  from (B1). The  $z$  statistic (12) of the Diebold–Mariano test of equal predictive ability of model  $j$  and model  $k$  is a multiple of the difference

$$\bar{S}^{(j)} - \bar{S}^{(k)}, \quad (\text{B6})$$

where  $S$  is the Poisson score. We proceed to prove the claims in (15) that the information gain  $\text{IG}_{(j,k)}$  and the information gain per earthquake  $\text{IG}_{(j,k)}^{\text{PE}}$  of model  $k$  over model  $j$  also are multiples of the Poisson score difference at (B6).

We start with time  $t$  fixed and consider the definition of the information gain in the purely spatial setting of Eq. (17) in Rhoades et al. (2011, p. 740). In this simpler setting, the information gain of model  $k$  over model  $j$  at time  $t$  is

$$\sum_{c=1}^C y_{c,t} \left( \log x_{c,t}^{(k)} - \log x_{c,t}^{(j)} \right) - \sum_{c=1}^C \left( x_{c,t}^{(k)} - x_{c,t}^{(j)} \right). \quad (\text{B7})$$

To see the equivalence of Eq. (B7) and Eq. (17) in Rhoades et al. (2011), note the specification of the quantity  $i_k$  at the top of their page 731 and the fact that

$$\sum_{c=1}^C y_{c,t} \left( \log x_{c,t}^{(k)} - \log x_{c,t}^{(j)} \right) = \sum_{z=1}^{\infty} z \sum_{c=1}^C \mathbb{1}(y_{c,t} = z) \left( \log x_{c,t}^{(k)} - \log x_{c,t}^{(j)} \right).$$

Summing the expression for the information gain at time  $t$  in (B7) over testing times  $t \in \{1, \dots, T\}$ , the spatio-temporal information gain  $\text{IG}_{(j,k)}$  of model  $k$  over model  $j$  is

$$\text{IG}_{(j,k)} = \sum_{t=1}^T \sum_{c=1}^C y_{c,t} \left( \log x_{c,t}^{(j)} - \log x_{c,t}^{(k)} \right) - \sum_{t=1}^T \sum_{c=1}^C \left( x_{c,t}^{(j)} - x_{c,t}^{(k)} \right). \quad (\text{B8})$$

Invoking Eqs. (9), (2), (1), and (B6), we see that the information gain  $\text{IG}_{(j,k)}$  is of the form stated in Eq. (15).

The expression for the information gain per earthquake  $\text{IG}_{(j,k)}^{\text{PE}} = \text{IG}_{(j,k)}/N_T$  in Eq. (15) is now immediate. We note that in the case of OEF-Italy, due to the overlap of the seven-day forecast periods, the earthquake count  $N_T$  equals seven times the number of unique target earthquakes in the catalog.

### B.3 Results for the CSEP T-test

As noted, the CSEP T-test of equal predictive ability of two models Rhoades et al. (2011, Section 2.3) is based on the information gain per earthquake

$$\text{IG}_{(j,k)}^{\text{PE}} = \frac{T}{N_T} \left( \bar{S}^{(j)} - \bar{S}^{(k)} \right),$$

of model  $k$  over model  $j$  as defined at (15). Rhoades et al. (2011) posit that under the null hypothesis of equal predictive ability the statistic

$$\Theta_{(j,k)} = N_T^{1/2} \frac{\text{IG}_{(j,k)}^{\text{PE}}}{s_{(j,k)}}, \quad (\text{B9})$$

where

$$s_{(j,k)}^2 = \frac{1}{N_T - 1} \sum_{t=1}^T \sum_{c=1}^C y_{c,t} \left( \Delta_{c,t}^{(j,k)} \right)^2 - \frac{1}{N_T(N_T - 1)} \left( \sum_{t=1}^T \sum_{c=1}^C y_{c,t} \Delta_{c,t}^{(j,k)} \right)^2$$

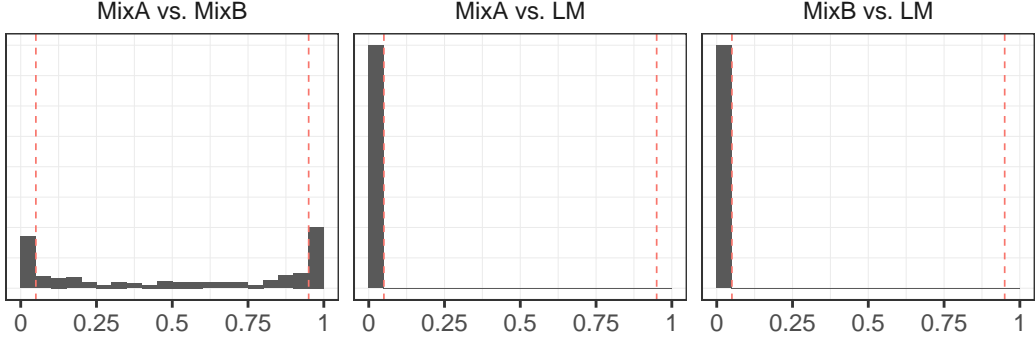


Figure B1: As Figure 5, but for the CSEP T-test.

Table B1: As Table 2, but for the CSEP T-test of the null hypothesis of equal predictive ability for CSEP Italy models. We show the respective information gain per earthquake ( $IG_{(j,k)}^{\text{PE}}$ , diagonal) from Table 3, the test statistic ( $\Theta_{(j,k)}$ , eq. (B9), above diagonal), and one-sided  $p$ -value (eq. (B10), below diagonal). Rows identify model  $j$  and columns model  $k$  in the test statistic at (B9).

	LRWA	LM	SMA	FCM	LG
LRWA	-0.053	5.304	11.337	15.677	28.277
LM	0.000	0.000	4.380	11.382	23.965
SMA	0.000	0.000	0.061	10.641	30.186
FCM	0.000	0.000	0.000	0.253	18.942
LG	0.000	0.000	0.000	0.000	0.925

and  $\Delta_{c,t}^{(j,k)} = \log x_{c,t}^{(j)} - \log x_{c,t}^{(k)}$ , has a Student- $t$  distribution with  $N_T - 1$  degrees of freedom. Unfortunately, this line of reasoning suffers from a neglect of the effects of spatio-temporal dependencies and the omission of terms associated to grid cells and time periods without target earthquakes. As a result, the one-sided  $p$  values generated by the T-test, namely,

$$p = 1 - \Psi_{N_T-1}(\Theta_{(j,k)}), \quad (\text{B10})$$

where  $\Psi_k$  denotes the CDF of the Student- $t$  distribution with  $k$  degrees of freedom, generally fail to be uniform between 0 and 1 when the null hypothesis is true.

We illustrate these issues in the simulation setting of Section 2.3. Figure B1 is the same as Figure 5 in Section 2.3, but now considering the CSEP T-test rather than the Diebold–Mariano test. The histogram at left in Figure B1 shows the  $p$  values that arise from 400 replicates of CSEP T-tests of Mix<sub>A</sub> (index  $j$ ) versus Mix<sub>B</sub> (index  $k$ ); we see that the histogram deviates considerably from the desired uniformity between 0 and 1.

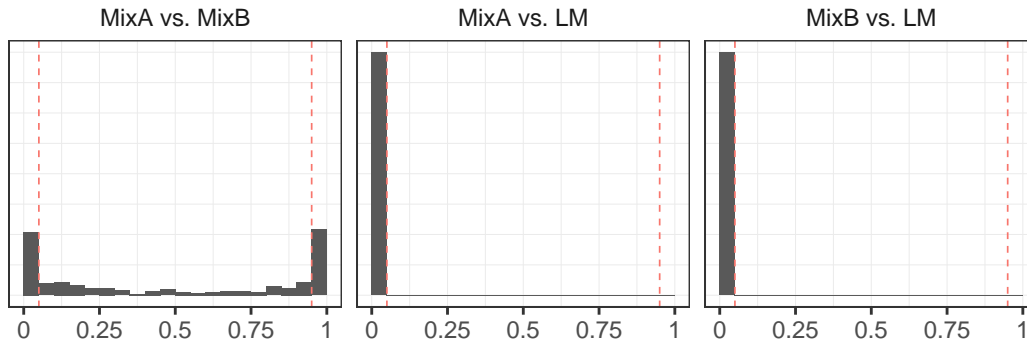


Figure B2: As Figure B1, but using forecasts on Mondays only.

Table B2: As Table B1, but using forecasts on Mondays only.

	LRWA	LM	SMA	FCM	LG
LRWA	-0.068	1.929	6.117	6.097	10.618
LM	0.027	0.000	1.777	4.650	8.549
SMA	0.000	0.038	0.070	3.964	10.664
FCM	0.000	0.000	0.000	0.266	6.731
LG	0.000	0.000	0.000	0.000	0.910

Specifically, 85 of the 400  $p$  values are smaller than 0.05, and 101 of them are larger than 0.95, rather than the nominal 20 under the null hypothesis. We conclude that the CSEP T-test rejects the null hypothesis of equal predictive ability more often than warranted. This behavior is mirrored in Table B1, where the T-test rejects the null hypothesis of equal predictive ability for every pair of the five CSEP Italy models.

One might speculate that the undesirable behavior under the null hypothesis stems from the overlap of the seven-day forecast periods in OEF-Italy. In this light, we repeat the analysis in Figure B2 and Table B2, but now considering forecasts issued on Mondays only, to avoid overlap in the seven-day forecast periods. Unfortunately, the aforementioned issues prevail. In the 400 tests of  $Mix_A$  versus  $Mix_B$ , 104 of the 400  $p$  values are smaller than 0.05, and 108 of them are larger than 0.95, rather than the nominal 20.

## C Generation of consistency bands for mean-reliability diagrams

To accommodate for the non-negative integer character of earthquake counts we use a resampling procedure based on Algorithm 3 in [Gneiting and Resin \(2023\)](#) for the generation of the consistency bands in Figures 6 and 7. The algorithm requires fully specified predictive distributions from which it then samples. In the setting at hand we have mean-forecasts (more specifically, expected counts) at our disposal only. To derive a fully specified predictive distribution from the mean-forecast at hand, we adapt the unconditional distribution of the number of observed earthquakes. Specifically, if the vector  $(p_0, p_1, \dots, p_m) \in [0, 1]^m$  comprises the empirical frequencies of observing  $0, 1, \dots, m$  earthquakes in the record at hand, we derive the predictive distribution  $F_x$  associated with the mean-forecast  $x$  as the discrete probability measure on  $0, 1, \dots, m$  with masses  $(p_0 + \varepsilon_x, p_1, \dots, p_m)/(1 + \varepsilon_x)$ , where  $\varepsilon_x$  is such that

$$x = \frac{1}{1 + \varepsilon_x} \sum_{j=1}^m j p_j, \tag{C1}$$

which ensures that the distribution  $F_x$  has mean  $x$ . Then we apply Algorithm 3 in [Gneiting and Resin \(2023\)](#) to the respective collection of pairs  $(F_x, x)$ .